공학석사 학위논문

UDR 을 위한 하드웨어 설계 연구

A Study on a Hardware Design for an Underwater Disk Robot

지도교수 최 형 식

2012 년 2 월

한국해양대학교 대학원

기 계 공 학 과

TRAN NGOC HUY

本 論文을 **Tran Ngoc Huy** 의 工學碩士 學位論文으로 認准함**.**

위원장 유삼상 (인)

위 원 최형식 (인)

위 원 김준영 (인)

2012 년 2 월

한국해양대학교 대학원

Acknowledgement

I would like to express my deep gratitude to my supervisor Professor Hyeung-Sik Choi, for his invaluable help, encouragement, and patience during the master course in Department of Mechanical Engineering. His insight, vision, suggestions, and special behavior of brisk style in work has impressed to me and helped me to archive success in research and study.

I am grateful to Professor Sam-sang You, major of Refrigeration, Air-conditioning and Energy System Engineering; Professor Joon-Young Kim, major of Marine Equipment Engineering; Professor Jae-hyun Jeong, major of Mechanical System Engineering... They all helped and taught me immeasurably in detailing comments for my study in Korea Maritime University, Korea.

Special thanks to all the members of Intelligent Robot & Automation Lab (KIAL) for giving me a helpful, active and comfortable environment which conducts my scientific pursuits.

I closely express my thanks to Korean and Vietnamese friends for their friendliness, sharing, and confidence.

Last but by no means least, it is warmly that I would like to thank my parents, my brother, and my sister for their constant support and encouragement.

Korea Maritime University, Pusan, Korea

February 1st 2012

Tran Ngoc Huy

A Study on a Hardware Design for an Underwater Disk Robot

Tran Ngoc Huy

Department of Mechanical Engineering
Graduate School of Korea Maritime University, 2012

Abstract

This paper introduces the new development of an Underwater Disk Robot (UDR) performing robust underwater motion under multi-directional disturbances. This is a new idea to overcome the underwater robot disadvantages which are motions, disturbance effect on the side. The UDR is six-DOF model composed of a frame structure include control system, sensor system ,four vertical actuators for heaving, rolling, pitching, rotating motion and three low-cost thrusters were developed for robust surging, swaying motion. Three thrusters are disposed symmetrically by 120 degrees to navigate along any directions by robust vector propulsion control scheme. The UDR is designed as a disk shaped vehicle to be less affected by external disturbances such as currents and waves. A control system including PID motion controller and sensor systems using depth sensor and low-cost AHRS sensor are developed.

Table of Contents

List of Tables

List of Figures

Chapter 1 Introduction

1.1Motivation

Ocean is cradle of life, treasury resource and transportation artery. In the 21st century, we will face three challenges, such as the contradiction between population explosion and limited living space, between exhausted land resource and growing requirement of social production, between eco-environmental degradation and human development. Beside that, there exist sea regions with dangerous mines that should be eradicated for humanitarian reasons. It is clearly convenient and useful to use underwater robots such as USV, ROV, AUV [1] for oceanographic, bathymetric survey costal area, support works of the underwater vehicles by aiding the communication, localization and mine countermeasures, with no risks for humans.

Remotely operated underwater vehicles (ROVs) are unoccupied, highly maneuverable underwater robots operated by a person aboard a surface vessel. They are linked to the ship by a group of cables that carry electrical signals back and forth between the operator and the vehicle. Most are equipped with at least a video camera and lights. Additional equipment is commonly added to expand the vehicle's capabilities. These may include a still camera, a manipulator or cutting arm, water samplers, and instruments that measure water clarity, light penetration, and temperature. The disadvantages of using an ROV include the fact that the human presence is lost, making visual surveys and evaluations more difficult, and the lack of freedom from the surface due to the ROV's cabled connection to the ship.

An autonomous underwater vehicle (AUV) is a robot which travels underwater without requiring input from an operator. It has two significant limiting factors. Firstly, batteries. Limitation in battery power restricted either endurance or the sensors that the vehicle could carry. Secondly, vehicle navigation and control.

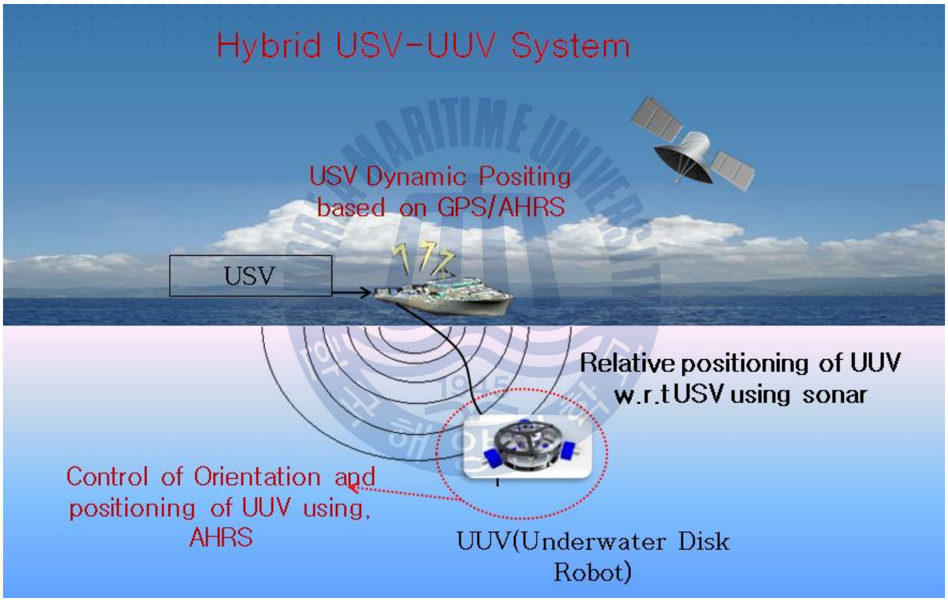

Fig. 1.1: Hybrid USV-UUV system.

Generally, the underwater vehicle either tend to be cumbersome and complex to run, or operationally simple, but not quite suitable platforms for deep water imaging and weak to side disturbance effects [2] [3] [4]. Aware of the currently existing capabilities of underwater robot, we have initially designed and developed Underwater Disk Robot (UDR) which has manned or unmanned ability, enable the operator to record imagery below the ocean surface. With the disk shape, symmetric redundant actuators and vector actuation system it can be the least side disturbance effect, robust underwater motion under multi-directional disturbances, swift motion to any directions such as horizontally, vertically and laterally.

1.2 Aim and Scope

In this study, it is desired to establish the modeling of UDR with symmetric structure and actuator's locations. The hardware system is designed to operate UDR by using DSP microcontroller, developed low-cost AHRS sensor. Further, it is aimed to control heaving, rolling, pitching, rotating motion through PID controller and Kalman filter.

Chapter 2 Modeling of the UDR

In this chapter, we describe the UDR's structure about actuators, sensors, control box, and shape. We define the equations governing the motion of the vehicle, analysis the vector actuation. These elements are addressed in the following sections.

2.1 Design UDR

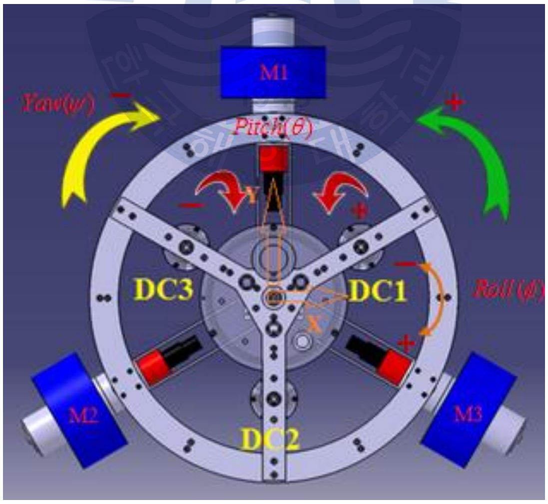

Fig. 2.1: 6 DOF motion.

The UDR is designed as a disk shaped vehicle (Figure 2.1) to be less affected by external disturbances such as currents, wave. Especially, with three thrusters disposed symmetrically by 120 degrees (Figure 2.2) are used to navigate along any directions by robust vector propulsion control scheme. They can control UDR for surging, swaying motion. And four vertical actuators which include three Z-cylinder DC Motors and RC Motor, perform for heaving, rolling, pitching, and rotating motion (Figure 2.3).

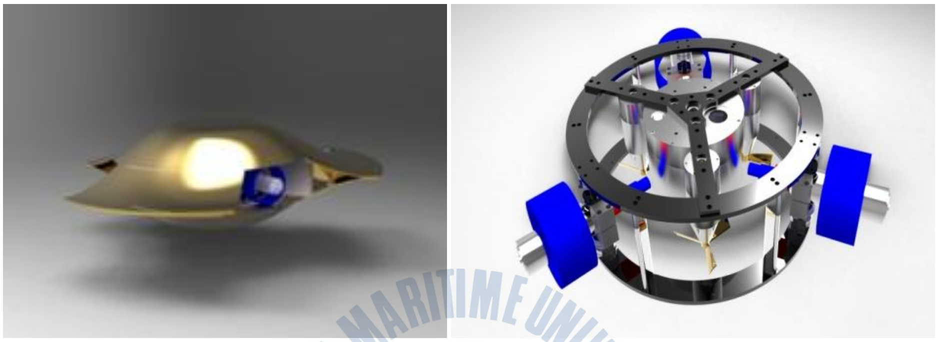

Fig. 2.2: 3D modeling of the UDR

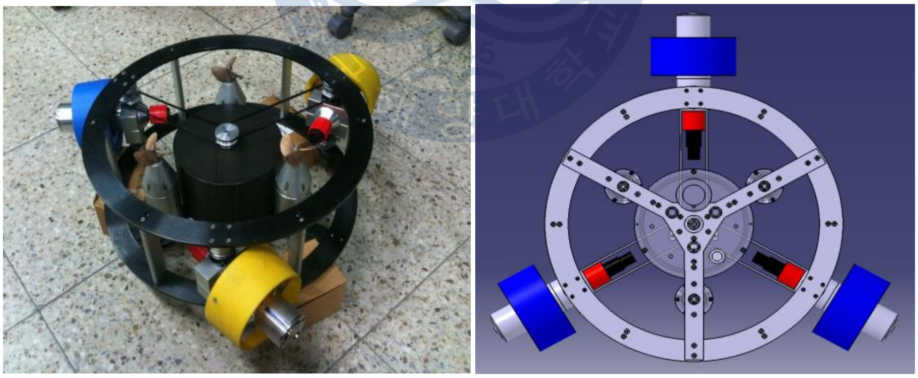

Fig. 2.3: Thrusters are disposed symmetrically by 120 degrees

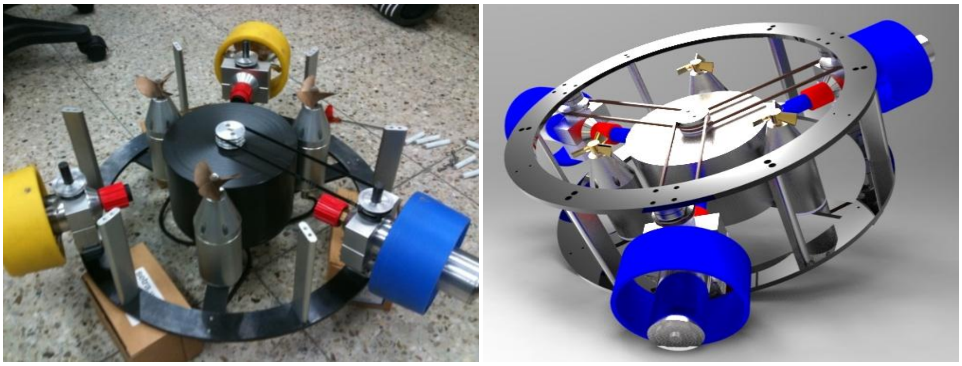

Fig. 2.4: The vertical actuators

The control box is designed to contain the RC motor (support in rotating motion), depth sensor, IMU sensor , and DSP board which is programmed for controlling UDR and communicate with computer (Figure 2.4). The below table 2.1 will show mechanism specification of the UDR.

Fig. 2.5: Control box

Table 2.1: Mechanism specification of the UDR

Parameter	Value
Weight	22kg
Diameter	0.475m
Height	0.177m
Depth	50m
Speed	2 knots (1.028m/s)
D.O.F	6

2.2 Elements of the governing equations

In this chapter, we define the equations governing the motion of the vehicle [5]. These equations consist of the following elements:

- Kinematics: the geometric aspects of motion
- Rigid-body Dynamics: the vehicle inertia matrix
- Mechanics: forces and moments causing motion

These elements are addressed in the following sections.

2.2.1 Vehicle Kinematics

The motion of the body-fixed frame of reference is described relative to an inertial or earth-fixed reference frame. The general motion of the vehicle in six degree of freedom can be described by the following vectors:

$$\begin{aligned} &\eta_1 = [x\ y\ z]^T; && \eta_2 = [\phi\ \theta\ \psi]^T \\ &v_1 = [u\ v\ w]^T; && v_2 = [p\ q\ r]^T \\ &\tau_1 = [X\ Y\ Z]^T; && \tau_2 = [K\ M\ N]^T \end{aligned} \tag{2.1}$$

Where:

- η describes the position and orientation of the vehicle with respect to the inertial or earth-fixed reference frame.
- v describes the translational and rotational velocities of the vehicle with respect to the body-fixed reference frame.
- τ describes the total forces and moments acting on the vehicle with respect to the body-fixed reference frame.

See Figure 2.6 for a diagram of the vehicle coordinate system.

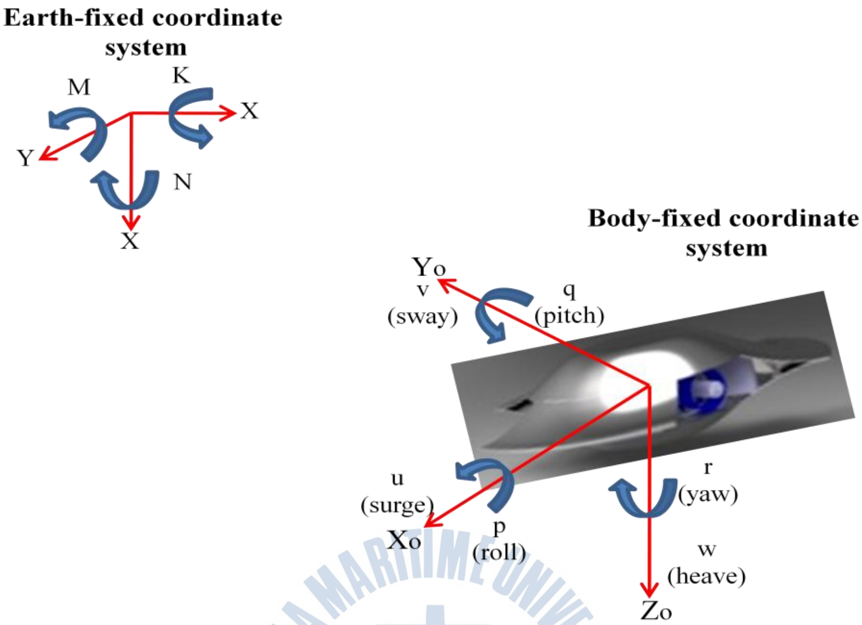

Fig. 2.6: UDR Body-fixed and Inertial Coordinate systems

The following coordinate transform relates translational velocities between body-fixed and inertial or earth-fixed coordinates:

$$\begin{bmatrix} \dot{x} \\ \dot{y} \\ \dot{z} \end{bmatrix} = J_1(\eta_2) \begin{bmatrix} u \\ v \\ w \end{bmatrix} \tag{2.2}$$

Where

$$J_1(\eta_2) = \begin{bmatrix} c\psi c\theta & -s\psi c\phi + c\psi s\theta s\phi & s\psi s\phi + c\psi s\theta c\phi \\ s\psi c\theta & c\psi c\phi + s\psi s\theta s\phi & -c\psi s\phi + s\psi s\theta c\phi \\ -s\theta & c\theta s\phi & c\theta c\phi \end{bmatrix} \tag{2.3}$$

Note that is $J_1(\eta_2)$ orthogonal:

$$(J_1(\eta_2))^{-1} = (J_1(\eta_2))^T \tag{2.4}$$

The second coordinate transform relates rotational velocities between body-fixed and earth-fixed cooridinates:

$$\begin{bmatrix} \dot{\phi} \\ \dot{\theta} \\ \dot{\psi} \end{bmatrix} = J_2(\eta_2) \begin{bmatrix} p \\ q \\ r \end{bmatrix} \tag{2.5}$$

Where

$$J_2(\eta_2) = \begin{bmatrix} 1 & s\phi t\theta & c\phi t\theta \\ 0 & c\phi & -s\phi \\ 0 & s\phi / c\theta & c\phi / c\theta \end{bmatrix} \tag{2.6}$$

Note that $J_2(\eta_2)$ is not defined for pitch angle $\theta = \pm 90^0$. This is not a problem, as the vehicle motion does not ordinarily approach this singularity. If we were in a situation where it became necessary to model the vehicle motion through extreme pitch angles, we could resort to an alternate kinematic representation such as quaternions or Rodriguez parameters.

2.2.2 Vehicle Rigid-body Dynamics

The locations of the vehicle centers of gravity and buoyancy are defined in terms of the body-fixed coordinate system as follows:

$$r_G = \begin{bmatrix} x_g \\ y_g \\ z_g \end{bmatrix} \qquad r_B = \begin{bmatrix} x_b \\ y_b \\ z_b \end{bmatrix} \tag{2.7}$$

In the following sections, we will show that the 6DOF nonlinear dynamic equations of motion can be conveniently express as:

$$M\dot{\upsilon} + C(\upsilon)\upsilon + D(\upsilon)\upsilon + g(\eta) = \tau \tag{2.8}$$

Where

M: Inertia matrix (including added mass)

$C(\upsilon)$: Matrix of Coriolis and centripetal terms (including added mass)

$D(\upsilon)$: Damping matrix

$g(\eta)$: Vector of gravitational forces and moments

τ: Vector of control inputs

The parameterization of the rigid-bod inertia matrix M

$$M = \begin{bmatrix} M_{11} & M_{12} \\ M_{21} & M_{22} \end{bmatrix} = \begin{bmatrix} mI_{3x3} & -mS(r_G) \\ mS(r_G) & I_0 \end{bmatrix} = \begin{bmatrix} m & 0 & 0 & 0 & mz_G & -my_G \\ 0 & m & 0 & -mz_G & 0 & mx_G \\ 0 & 0 & m & my_G & -mx_G & 0 \\ 0 & -mz_G & my_G & I_x & -I_{xy} & -I_{xz} \\ mz_G & 0 & -mx_G & -I_{yz} & I_y & -I_{yz} \\ -my_G & mx_G & 0 & -I_{zx} & -I_{zy} & -I_z \end{bmatrix} \tag{2.9}$$

We can always parameterize the Coriolis and centripetal matrix by defining:

$$C(\upsilon) = \begin{bmatrix} 0_{3x3} & -S(M_{11}\upsilon_1 + M_{12}\upsilon_2) \\ -S(M_{11}\upsilon_1 + M_{12}\upsilon_2) & -S(M_{21}\upsilon_1 + M_{22}\upsilon_2) \end{bmatrix}$$
$$= \begin{bmatrix} 0 & 0 & 0 & m(y_G q + z_G r) & -m(x_G q - w) & -m(x_G r + v) \\ 0 & 0 & 0 & -m(y_G p + w) & m(z_G r + x_G p) & -m(y_G r - u) \\ 0 & 0 & 0 & -m(z_G p - v) & -m(z_G q + u) & m(x_G p + y_G q) \\ -m(y_G q + z_G r) & m(y_G p + w) & m(z_G p - v) & 0 & -I_{yz} q - I_{xz} p + I_z r & I_{yz} r + I_{xy} p - I_y q \\ m(x_G q - w) & -m(z_G r + x_G p) & m(z_G q + u) & I_{yz} q + I_{xz} p - I_z r & 0 & -I_{xz} r - I_{xy} q + I_x p \\ m(x_G r + v) & m(y_G r - u) & -m(x_G p + y_G q) & -I_{yz} r - I_{xy} p + I_y q & I_{xz} r + I_{xy} q - I_x p & 0 \end{bmatrix} \tag{2.10}$$

Given that the origin of the body-fixed coordinate system is located at the center of buoyance.Form equation (2.8) we have the equations of motion for a rigid body in six degrees of freedom, defined in terms of body-fixed coordinates:

$$
\begin{aligned}
&m[\dot{u} - vr + wq - x_g(q^2 + r^2) + y_g(pq - \dot{r}) + z_g(pr + \dot{q})] = \sum X_{ext} \\
&m[\dot{v} - wp + ur - y_g(r^2 + p^2) + z_g(pr - \dot{p}) + x_g(qp + \dot{r})] = \sum Y_{ext} \\
&m[\dot{w} - uq + vp - z_g(p^2 + q^2) + x_g(rp - \dot{q}) + y_g(rq + \dot{p})] = \sum Z_{ext} \\
&I_{xx}\dot{p} + (I_{zz} - I_{yy})qr - (\dot{r} + pq)I_{xz} + (r^2 - q^2)I_{yz} + (pr - \dot{q})I_{xy} \\
&\qquad + m[y_g(\dot{w} - uq + vp) - z_g(\dot{v} - wp + ur)] = \sum K_{ext} \\
&I_{yy}\dot{q} + (I_{xx} - I_{zz})rp - (\dot{p} + qr)I_{xy} + (p^2 - r^2)I_{xz} + (qp - \dot{r})I_{yz} \\
&\qquad + m[z_g(\dot{u} - vr + wq) - x_g(\dot{w} - uq + vp)] = \sum M_{ext} \\
&I_{zz}\dot{r} + (I_{yy} - I_{xx})pq - (\dot{q} + rp)I_{yz} + (q^2 - p^2)I_{xy} + (rq - \dot{p})I_{xz} \\
&\qquad + m[x_g(\dot{v} - wp + ur) - y_g(\dot{u} - vr + wq)] = \sum N_{ext}
\end{aligned} \tag{2.11}
$$

Where m is the vehicle mass. The first three equations represent translational motion, the second three rotational motion. Note that these equations neglect the zero-valued center of buoyancy terms.

Given the body-fixed coordinate system centered at the vehicle center of buoyancy, we have the following, diagonal inertia tensor.

$$
I_o = \begin{bmatrix} I_{xx} & 0 & 0 \\ 0 & I_{yy} & 0 \\ 0 & 0 & I_{zz} \end{bmatrix} \tag{2.12}
$$

This is based on the assumption, I_{xy}, I_{xz}, and I_{yz} are small compared to the moments of inertia I_{xx}, I_{yy}, and I_{zz}.

This simplifies the equations of motion to the following:

$$
\begin{aligned}
m[\dot{u}-vr+wq-x_g(q^2+r^2)+y_g(pq-\dot{r})+z_g(pr+\dot{q})] &= \sum X_{ext} \\
m[\dot{v}-wp+ur-y_g(r^2+p^2)+z_g(pr-\dot{p})+x_g(qp+\dot{r})] &= \sum Y_{ext} \\
m[\dot{w}-uq+vp-z_g(p^2+q^2)+x_g(rp-\dot{q})+y_g(rq+\dot{p})] &= \sum Z_{ext} \\
I_{xx}\dot{p}+(I_{zz}-I_{yy})qr+m[y_g(\dot{w}-uq+vp)-z_g(\dot{v}-wp+ur)] &= \sum K_{ext} \\
I_{yy}\dot{q}+(I_{xx}-I_{zz})rp+m[z_g(\dot{u}-vr+wq)-x_g(\dot{w}-uq+vp)] &= \sum M_{ext} \\
I_{zz}\dot{r}+(I_{yy}-I_{xx})pq+m[x_g(\dot{v}-wp+ur)-y_g(\dot{u}-vr+wq)] &= \sum N_{ext}
\end{aligned} \tag{2.13}
$$

2.2.3 Vehicle Mechanics

In the vehicle equations of motion, external forces and moments are included:

$$\sum F_{ext} = F_{hydrostatic} + F_{lift} + F_{drag} + F_{control} \tag{2.14}$$

These forces are described in terms of vehicle coefficients. They are based on a combination of theoretical equations and empirically-derived formulae.

2.3 Vector actuation analysis

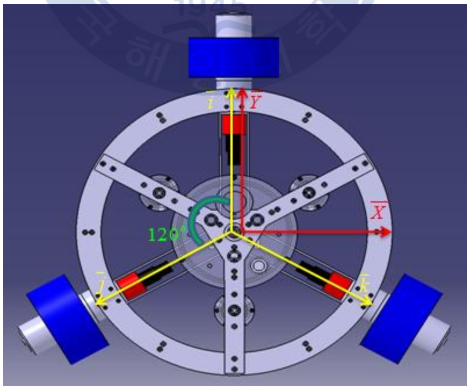

Fig. 2.7: The unit vector.

Three thrusters make the forces: $\overrightarrow{F_i}, \overrightarrow{F_j}, \overrightarrow{F_k}$

The total force: $\overrightarrow{F} = F_X.\overrightarrow{X} + F_Y.\overrightarrow{Y}$

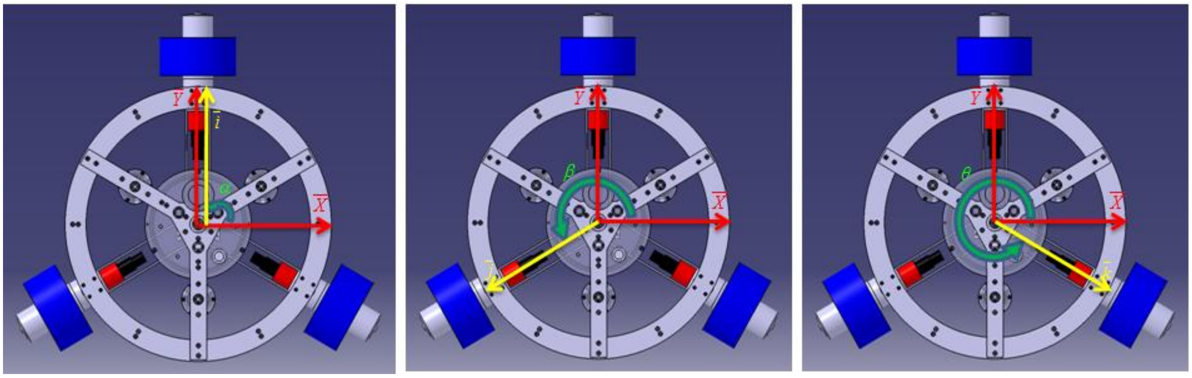

Fig. 2.8: Vector actuation analysis.

The unit vector:

$$\vec{i} = \cos\alpha.\vec{X} + \sin\alpha.\vec{Y}$$
$$\vec{j} = \cos\beta.\vec{X} + \sin\beta.\vec{Y} \quad (2.15)$$
$$\vec{k} = \cos\theta.\vec{X} + \sin\theta.\vec{Y}$$

The total force effect to UDR:

$$\vec{F} = \vec{F_i} + \vec{F_j} + \vec{F_k}$$

$$F_X.\vec{X} + F_Y.\vec{Y} = F_i.\vec{i} + F_j.\vec{j} + F_k.\vec{k}$$

$$= F_i(\cos\alpha.\vec{X} + \sin\alpha.\vec{Y}) + F_j(\cos\beta.\vec{X} + \sin\beta.\vec{Y}) + F_k(\cos\theta.\vec{X} + \sin\theta.\vec{Y})$$

$$= (F_i.\cos\alpha + F_j.\cos\beta + F_k.\cos\theta)\vec{X} + (F_i.\sin\alpha + F_j.\sin\beta + F_k.\sin\theta)\vec{Y} \quad (2.16)$$

$$\Rightarrow \begin{cases} F_X = F_i.\cos\alpha + F_j.\cos\beta + F_k.\cos\theta \\ F_Y = F_i.\sin\alpha + F_j.\sin\beta + F_k.\sin\theta \end{cases}$$

$$\Rightarrow \begin{bmatrix} F_X \\ F_Y \end{bmatrix} = \begin{bmatrix} \cos\alpha & \cos\beta & \cos\theta \\ \sin\alpha & \sin\beta & \sin\theta \end{bmatrix} \begin{bmatrix} F_i \\ F_j \\ F_k \end{bmatrix}$$

Chapter 3 Hardware Design

In this chapter, we will explain about UDR system. There are DSP micro-controller, actuators (Thrusters, RC Motor, DC Motors), motor driver, and sensors (depth, AHRS). The AHRS is developed and applied to control system.

3.1 Microcontroller

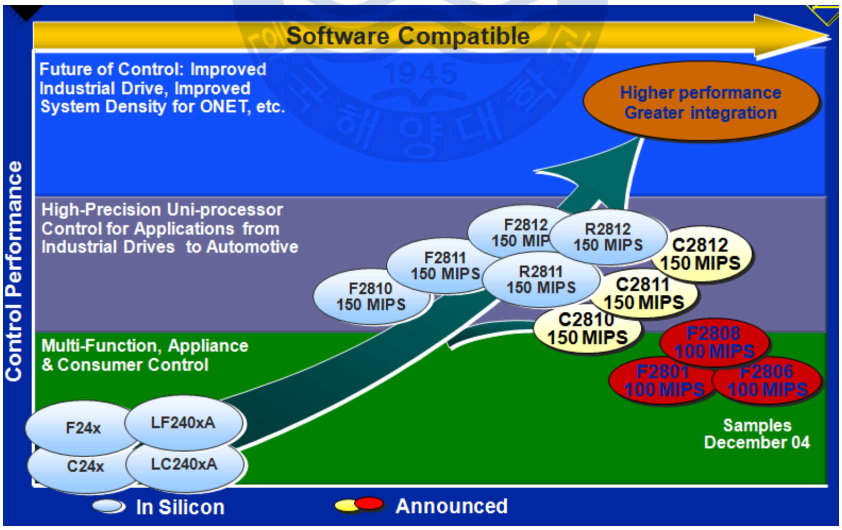

Fig. 3.1: Roadmap of TMS320C2000 DSC's.

Ti's C2000 devices [6] are 32 bit microcontrollers with high performance integrated peripherals designed for real-time control applications. Its math-optimized core gives designers the means to improve system efficiency, reliability, and flexibility. Powerful integrated peripherals make C2000 devices the perfect single-chip control solution. C2000's development tools strategy and software create an open platform with the goal of maximizing usability and minimizing development time.

C2000 apllications:

- Digital motor control
- Renewable energy systems
- Digital power conversion
- Adaptive lighting systems
- Automotive applications
- Power line communications etc.

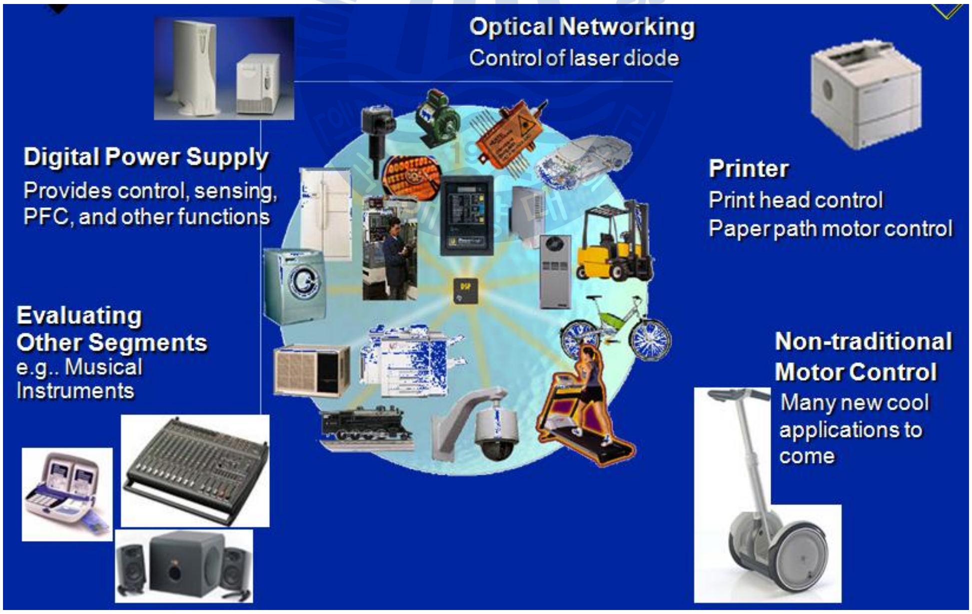

Fig. 3.2: Broad C28x Application Base.

In UDR, we used two kind of DSP: TMS320F28335 and TMS320F2812. The device nomenclature decoder is shown by following figure.

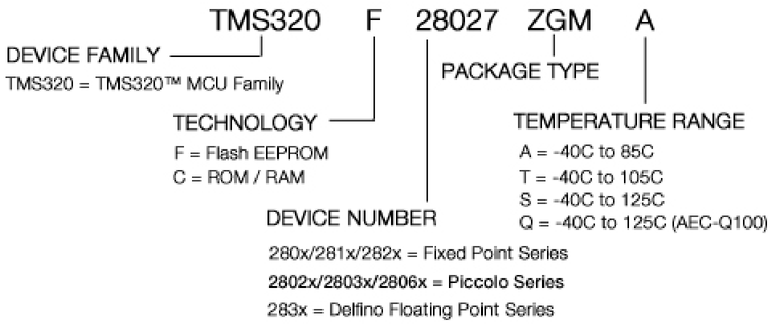

Fig. 3.3: The DSP nomenclature decoder.

Table 3.1: Specifications of DSP.

Parameter	**F28335**	**F2812**
CPU	32 bit	32 bit
Floating-point Unit	√	
MIPS	150	150
RAM (words)	34K	18K
ROM (words)		
Flash (words)	256K	128K
BootROM (words)	8K	4K
CAP/QEP	6/2	6/6
PWM	18	16
TIMER	3	7
ADC Resolution	12-bit	12-bit
Channels	16	16
Conv time	80ns	200ns
McBSP	√	√
EXMIF	√	√
Watch Dog	√	√
SPI	√	√
SCI (UART)	3	2
CAN	2	2
Volts (V)	3.3 I/O	3.3 I/O
# I/O	88	56
Package	176 LQFP 179 BGA	176 LQFP 179 BGA

3.2 Actuators and Equipments

3.2.1 DC Motor

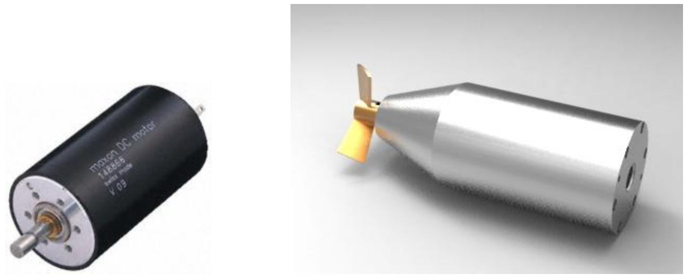

Fig. 3.4: Maxon DC motor.

Specifications:

Nominal Voltage :	24V
No load speed :	8810rpm
No load current :	164mA
Nominal torque :	1020mNm
Terminal inductance :	0.119mH
Power :	60W
Weight of motor :	238g

Motor driver

We designed DC Motor driver which was based on H-bridge circuit.

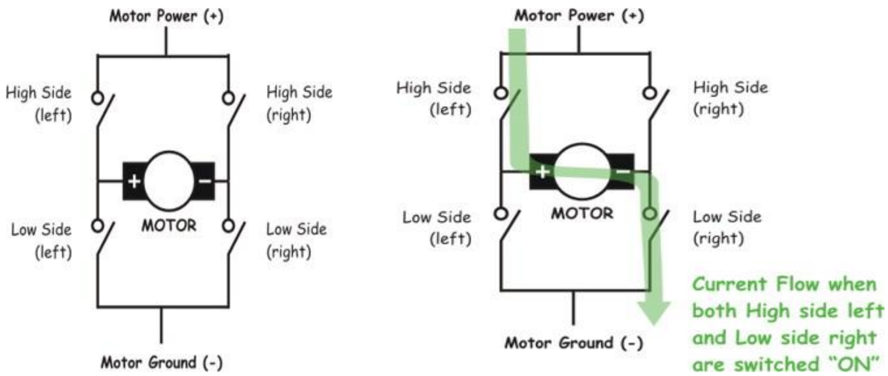

Fig. 3.5: H-bridge circuit.

Table 3.2: Summarize H-bridge operation.

High side left	High side right	Lower left	Lower right	Description
On	Off	Off	On	Clockwise
Off	On	On	Off	Counter-clockwise
On	On	Off	Off	Brake
Off	Off	On	On	Brake

Motor motion controller is shown in Fig, and Ti's TMS320F2812 processor controls the motor driver that consists of 500W total for two DC servo motor. In addition, with the built current sensor in motor driver we can apply PID control algorithm and the trapezoidal speed method.

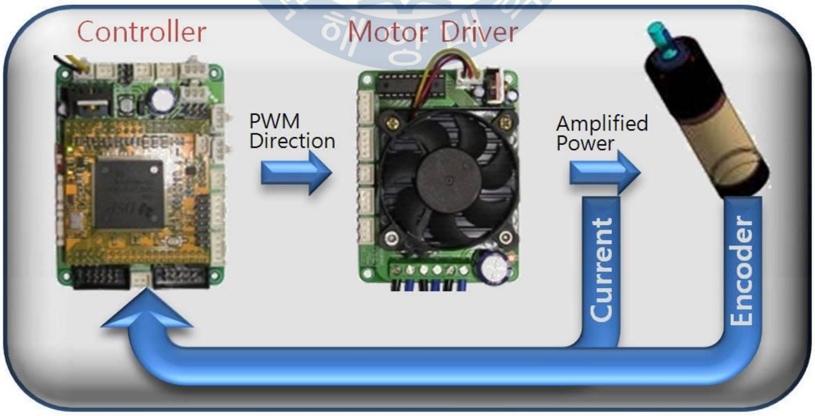

Fig. 3.6: DC motor motion control system.

Specifications:

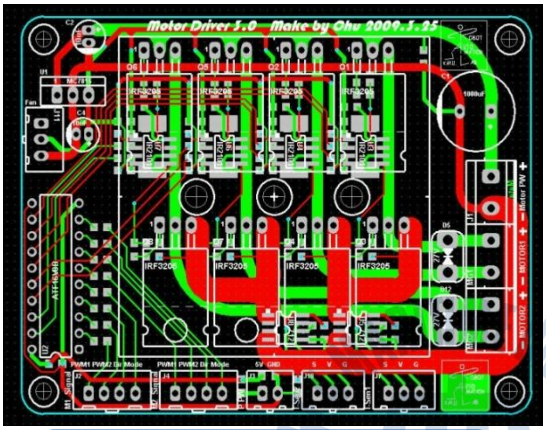

DSP Extension Board

Input:

- 24V or 5V Main Power
- 4 ADC
- 14 IO
- 2 External Input
- 2 Encoder signal

Output:

- 0.5% accurate 5V for sensor reference
- 5V - 1A
- 10 PWM
- 14 IO Output(Include PWM Output)

Communication:

- 2 SCI
- CAN Bus

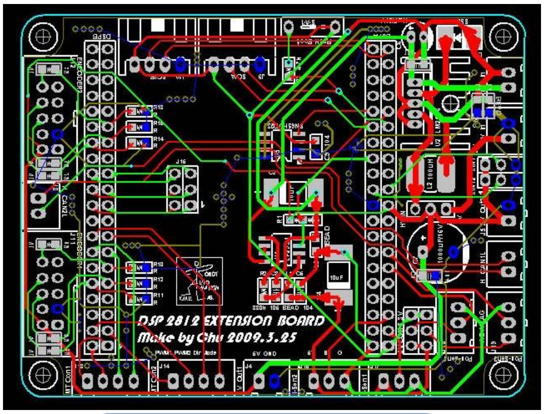

Motor Driver

Specification:

- 10~24V Dual DC Motor driver
- Up to 500W DC Motor drive enable
- 20A max current analog data output
- User programmable drive input
- 60 X 80mm size
- Fan heat sink

Fig. 3.7: Specifications of DC Motor Driver.

3.2.2 RC Motor (Dynamixel RX-64)

Dynamixel is a robot-only Smart Actuator with a new concept integrating speed reducer, controller, driver, network function, etc. into one module.

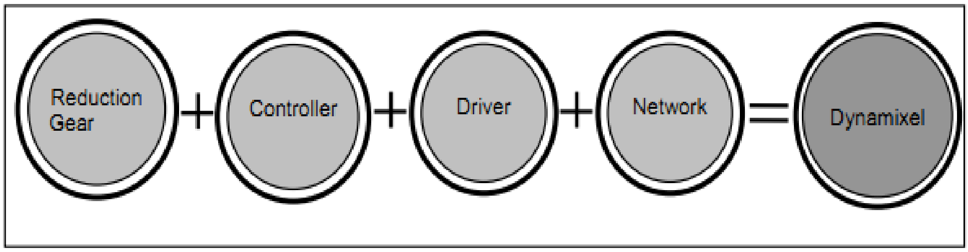

Fig. 3.8: Define Dynamixel RX-64.

Fig. 3.9: Dynamixel RC motor.

Strong points of Dynamixel:

- Torque: In spite of the compact size, it generates relatively big Torque by way of the efficient speed reduction

- Close control: It can control location and speed with the resolution of 1024
- Elasticity setting: It can set up the extent of elasticity when controlling position with compliance driving.
- Position, speed: It can read the current position and speed
- Communication: Dynamixel with a unique ID is controlled by packet communication on a BUS and supports networks such as TTL, RS485, and Can depending on the type of model.
- Distribution control: Since the main processor can set speed, position, compliance, torque, etc. simultaneously with a single command packet.
- Safety device: Is has the function, which notifies when internal temperature, torque, supplied voltage, etc. deviate from what the user has set, and the function, which allows it to cope with situation by itself.

Table 3.3: Specifications of RX-64

Parameter	RX-64	
Weight (g)	125	
Dimension (mm)	40.2x61.1x41.0	
Gear reduction ratio	1/200	
Applied voltage (V)	At 15V	At 18V
Final reduction stopping torque (kgf.cm)	64.4	77.2
Speed (sec/60 degrees)	0.188	0.157

Resolution: 0.29^0

Running degree: 300^0, Endless Turn

Voltage: 12V-21V

Max Current:	1200mA
Running Temp:	$-5^0C\_+85^0C$
Command signal:	Digital Packet
Protocol:	RS485 Asynchronous Serial Communication (8bit,

1stop, No parity)

Link:	RS485 Multi Drop Bus
ID:	254 ID (0_253)
Communication Speed:	7343 bps_1 Mbps
Sensing & measuring:	Position, Temperature, Load, Input Voltage, etc.
Material Quality:	Full metal gear, engineering plastic body
Motor:	Maxon RE-MAX
Standby current:	50mA

3.2.3 Thruster

We developed the 300w underwater thrusting system driven by a brushless DC (BLDC) motor for underwater robots. A design of the structure such as the structure analysis on the thrusting system using FEM and the design of the propeller using the fluid analysis has been performed. The performance test of the designed and developed thrusting system in water and in air was undertaken and its results were compared with an existing product with high performance. The comparison results show that the developed thrusting system has better performance by 16% in forward thrusting force and by 12% in backward thrusting force (Table 3.5) [7]. Also, a new structure such as decoupling and non-gear structure has been developed with characteristics in table 3.4.

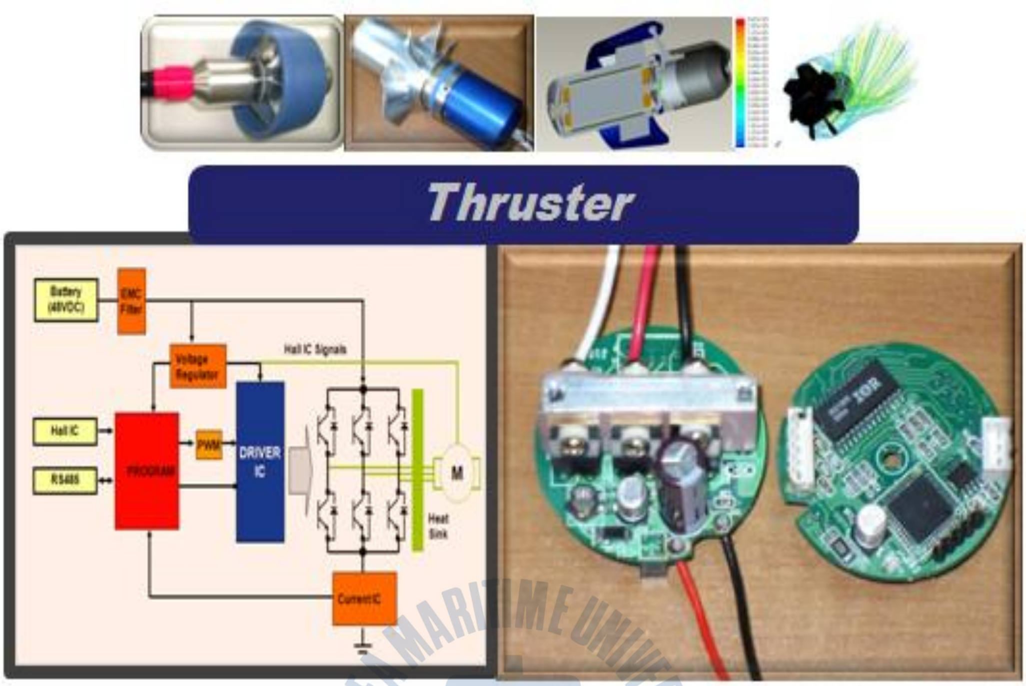

Fig. 3.10: BLDC driver.

Specifications

	units	Motor Data
input power	W	300
maxium speed	rpm	2000
weight	kg	1.3
pressure resistance	atm	50
forward thrusting force	kg	5
backward thrusting force	kg	2.5
torque	kg.cm	15
efficiency	%	60
Reduction		gearless
rotor type		outer rotor

Fig. 3.11: Specification of developed thrusting system.

Table 3.4: Comparison with present products.

Division	Power transmission structure	Characteristics
Present products	Motor + Gear + Magnetic coupling	Complex, good sealing, light, small
	Motor + Magnetic coupling	Complex
	Motor + Gear + sealer	Complex, bad sealing
	Motor + sealer	Simple, bad sealing
Developed system	Magnetic outer rotor + can	Simple, good, sealing, heavy

Table 3.5: Thrust test results.

Forward Direction			Backward Direction		
No.	rpm	Thrust (N)	No.	rpm	Thrust (N)
1	626	4.12	1	549	0.98
2	845	5.00	2	655	2.55
3	975	10.79	3	749	4.12
4	1084	13.93	4	864	8.04
5	1152	15.70	5	968	11.18
6	1200	19.62	6	1056	13.24
7	1251	21.97	7	1132	14.22
8	1289	24.03	8	1185	14.91
9	1291	25.51	9	1215	15.70
10	1324	26.98	10	1242	16.87

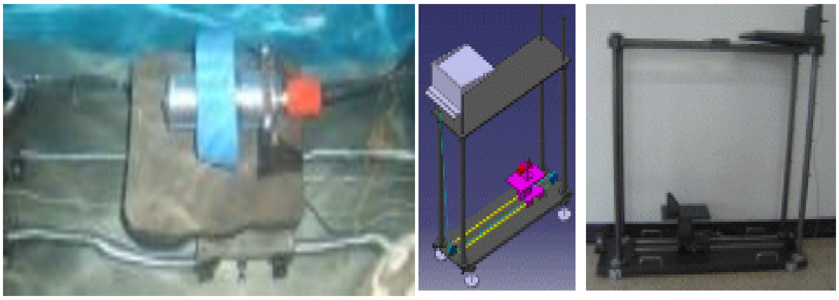

Fig. 3.12: Configuration of experimental apparatus.

3.3 Sensor

3.3.1 Model PSH (high performance pressure transducer)

PSH model is high precise and its media-wetted materials are composed of stainless steel 316L, having excellent corrosion-resistant properties. It is applied to precise measurement and builds an inner amplifier to interface with various kinds of controllers.

Applications:

- Process control
- Hydraulics & Pneumatic
- Compressor control
- Chillers
- Refrigeration equipment

Fig. 3.13: Model PSH.

Specifications:

- Range: 0-2 kgF/cm^2
- Voltage: 1-5VDC
- Accuracy: ±0.15%FS
- Thermal effect on zero: ±0.03%FS/C
- Operating temperature range: $-20 \sim 80^{0}C$
- Weight:140g

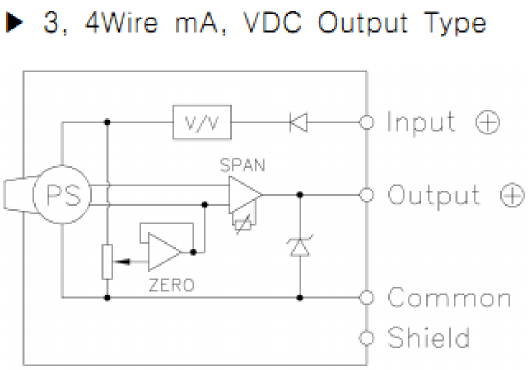

Fig. 3.14: Internal circuit diagram of pressure sensor.

3.3.2 Developed AHRS

a. Purpose of developing AHRS :

- Fields of use in robotics, aerospace, autonomous vehicle, marine industry.
- Develop a low-cost system while still keep high accuracy.
- Initiatively keep technology and develop, integrate into another applications flexibly.

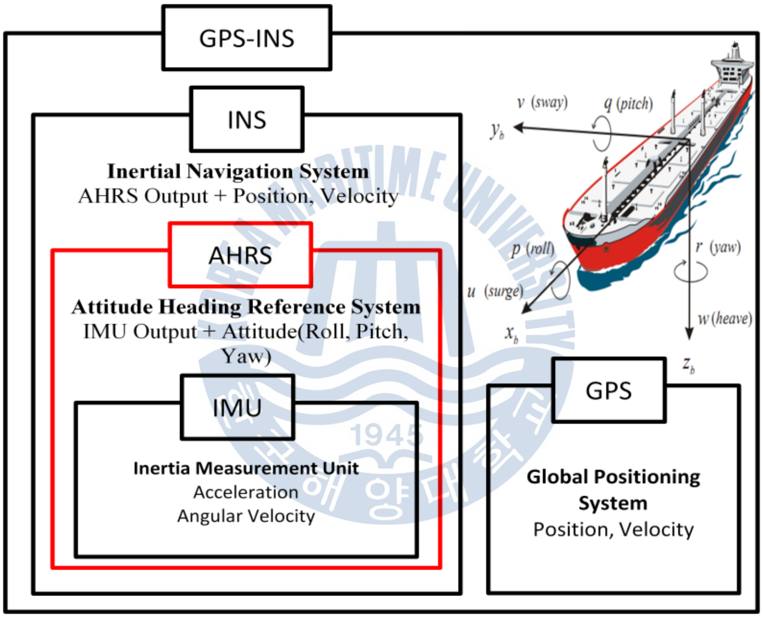

Fig. 3.15: Attitude heading reference system.

Design Attitude heading reference system:

Each method which determines attitude and heading has advantages and disadvantages. The method using rate gyro has good performance in short time but results in drift after long period. Meanwhile, the method using accelerometer has good performance when the body is under non-acceleration state but is invalid when the body is accelerating. The method using magnetometer has no drift but is valid only in the homogeneous and undisturbed Earth's magnetic field. Therefore, a fusion method is necessary to exploit advantages of each method. [8]

b. Hardware design process

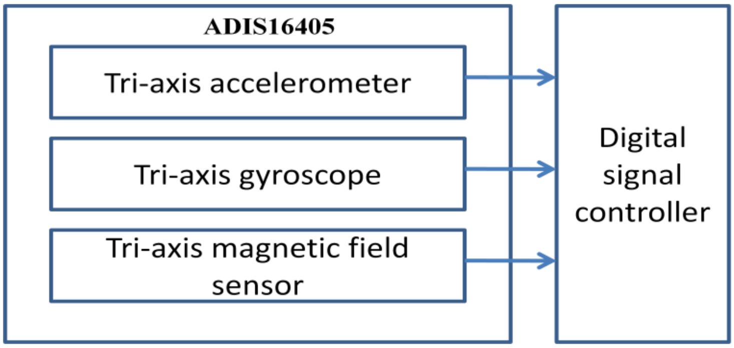

Fig. 3.16: Attitude heading reference system block schematic.

In our approach, the tri-axis inertial sensor with magnetometer ADIS16405 which is a product of Analog Devices, Inc. are used. Signals coming from the sensor are processed by digital signal controller TMS320F28335 where Kalman filter and data fusion algorithm are implemented. A prototype PCB is developing as illustrated in following figure 3.21.

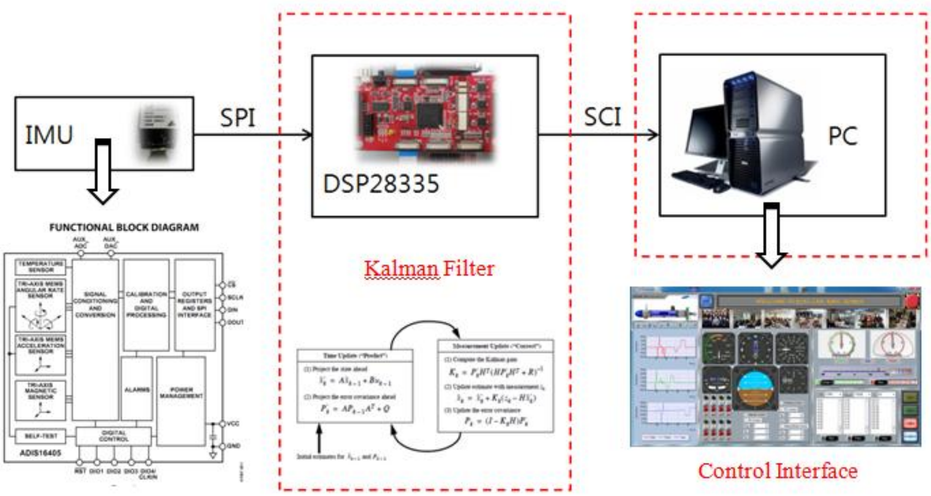

Fig. 3.17: Prototype board in development process.

- **ADIS16405 sensor:**

The ADIS16405 sensor is a complete inertial system that includes a tri-axis gyroscope, a tri-axis accelerometer, and a tri-axis magnetometer. The ADIS16405 combines industry-leading MEMS technology with signal conditioning that optimizes dynamic performance. This sensor provides a simple, cost-effective method for integrating accurate, multi-axis inertial sensing into industrial systems, especially when compared with the complexity and investment associated with discrete designs. An improved SPI interface and register structure provide faster data collection and configuration control.

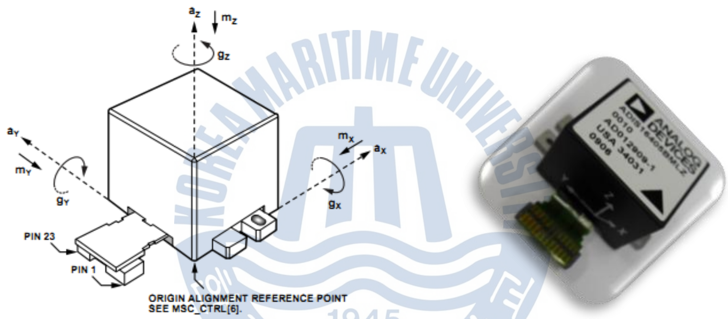

Fig. 3.18: Axial Orientation.

Specifications:

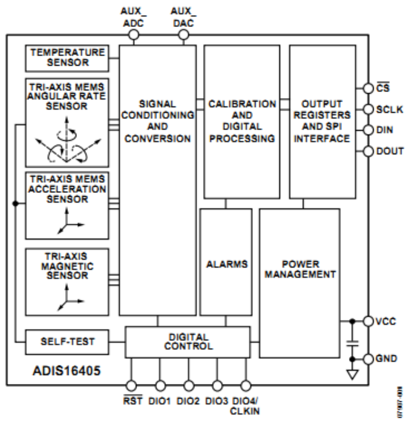

- Tri-axis, digital gyroscope ±75°/sec, ±150°/sec, ±300°/sec
  Output noise : 0.9 °/sec
- Tri-axis, ±18g digital accelerometer
  Output noise : 9 m*g*
- Tri-axis, ± 2.5gauss digital magnetometer
  Output noise : 1.25 mgauss
- Digitally controlled sampled rate up to 819.2SPS
- Operating temperature range: -40℃ to +105℃

Fig. 3.19: Functional block diagram.

- **Prototype PCB:**

The most important element in using kalman Filter is real time. So the collection of microcontroller is necessary to satisfy it. Digital signal controller TMS320F28335 with frequency up to 150MHz is chose. It is connected with sensor through SPI interface, and transfer attitude data to computer by using serial port.

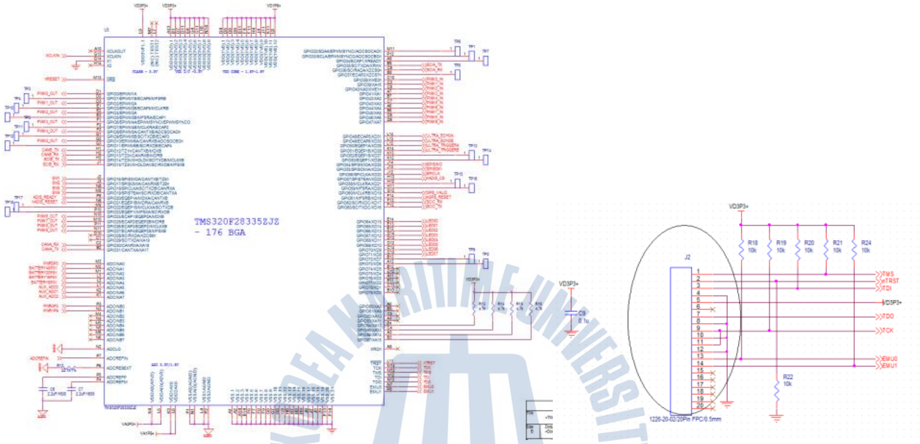

Fig. 3.20: TMS320F28335 pins, SPI port.

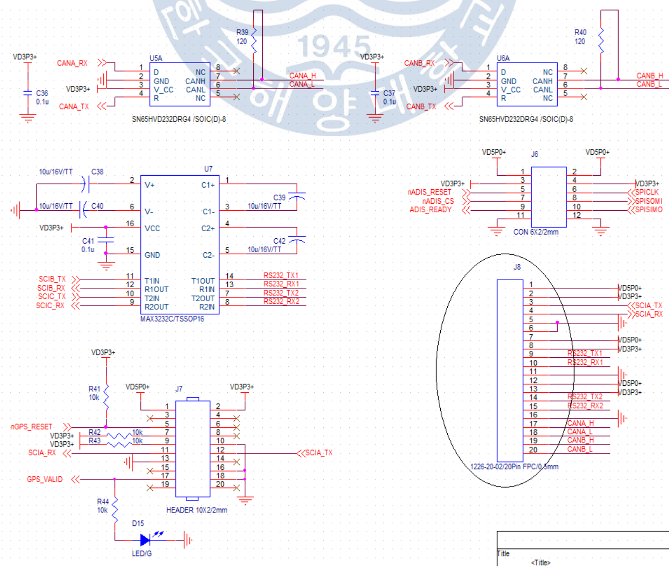

Fig. 3.21: CAN and Serial port.

- **AHRS’s Interface:**

The AHRS’s interface is designed by Visual Studio 2008. It is one of powerful tools for making Graphical Application Programming Interface (API) which is useful, flexible, eye-catching… By using this interface, we can easily setup and supervise the AHRS.

Fig. 3.22: AHRS’s Interface.

c. Control algorithm and experiments:

In first 10 seconds, use Low-Pass filter to get the average Euler Angles with frequency 50Hz. The initial Quaternion of Kalman filter loop is calculated from the average Euler Angles. After every loop cycle, converting Euler Angles from Quaternion, we will have the attitude of body. Kalman filter will be discussed more extensively later in the chapter 4.

3.4 UDR System

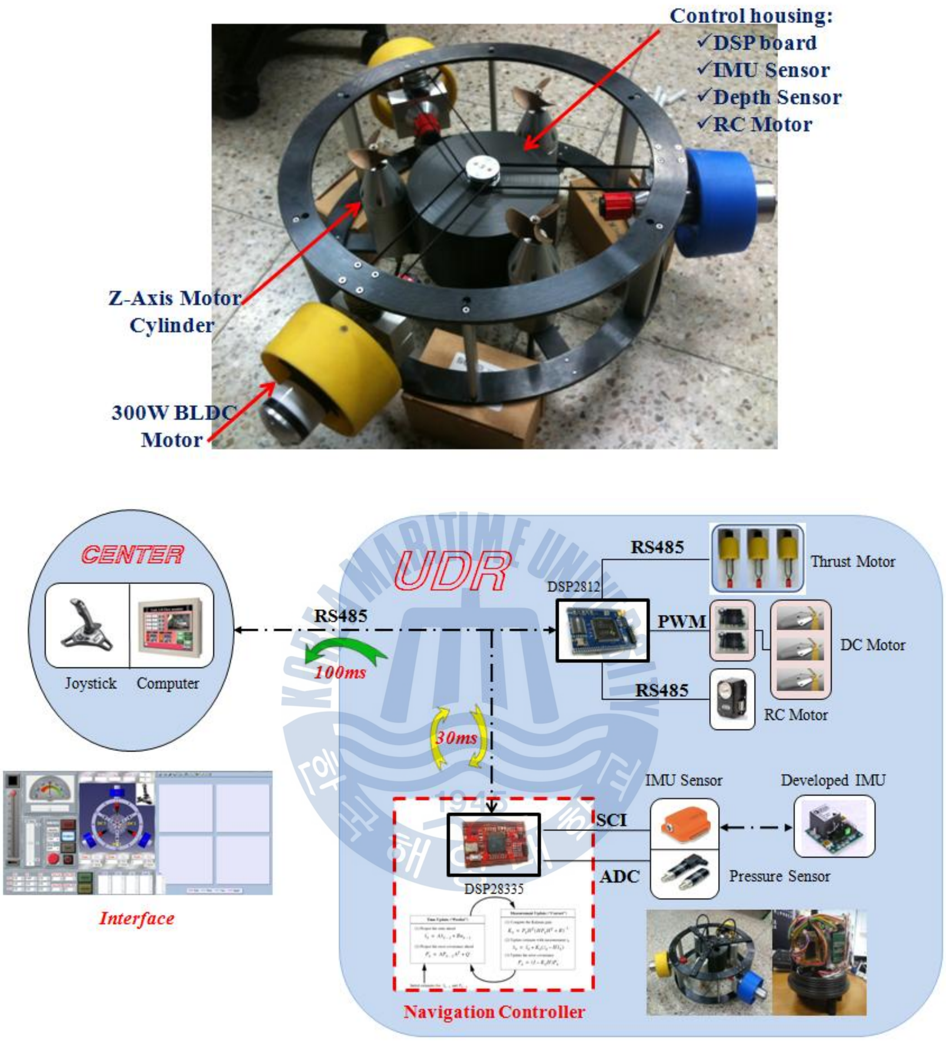

Fig. 3.23: UDR system diagram.

- The UDR control system is built by computer interface which has functions such as UDR action supervision, give control command, set up PID Parameters: Kp, Ki, Kd, draw plots and connect with UDR by using RS485 communication every 100ms.

- Controller board: control 3 Thrusters_48V by RS485 communication with bandrate 38400bps ,3 DC Motor_24V by DC Motor Driver and RC Motor with baudrate 115200bps
- Sensor board: collect the attitude signals through using Kalman Filter: roll (defined from $[-180^0 ... 180^0]$), pitch(defined from $[-90^0 ... 90^0]$), yaw (defined from $[-180^0 ... 180^0]$), linear acceleration accX, accY, accZ, and depth of UDR.

The Controller board will send command and will receive UDR's attitude signals from sensor board every 30ms. After having data, DSP2812 will apply PID Algorithm to control UDR to desired position, attitude …

Chapter 4 Theoretical Background

In this chapter, we will review the theoretical background that are the Attitude and Heading representation, Kalman filter, and Proportional Integral Differential (PID) control.

4.1 Attitude and Heading representation

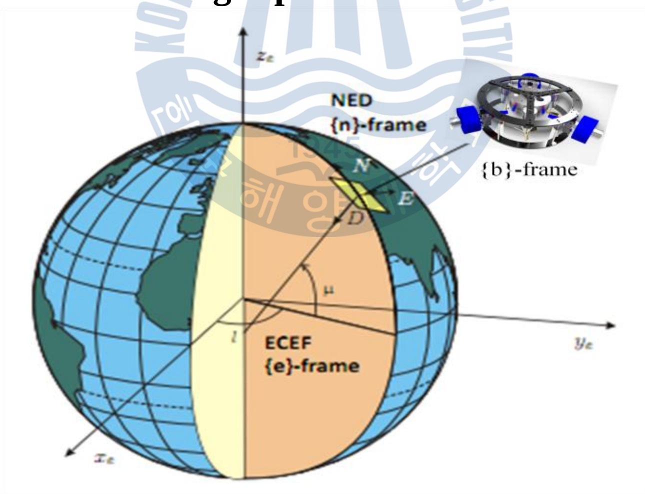

Fig. 4.1: Reference frames.

Before describing the attitude and heading estimation system, we should agree on how attitude and heading angles are represented. Consider a rigid body rotating and translating in the inertial space. Our aim is to estimate attitude and heading of the rigid body in the inertial space. To do this, three right-handed orthogonal coordinate frames are defined [9]

- Navigation frame (n-frame): It was used as reference frame. The n-frame has its origin at some point in the body where the measurement system is located. With x_n-axis points North, y_n-axis points East and z_n-axis points vertical down to the Earth's centre. It is so called North-East-Down (NED) frame.
- Body frame (b-frame): Moving coordinate frame fixed to the body. With the x_b-axis (roll) points forward, y_b-axis (pitch) points to the right and the z_b-axis (yaw) points downward
- Horizontal frame (h-frame): The b-frame is called the h-frame when their attitude angles are zeros.

Various mathematical representation can be used to define the attitude and heading of a body frame with respect to a reference frame such as: direction cosine matrix, Euler angles, Quaternion.

a) Euler Angles: It is utilized because of its intuitive nature and popularity despite drawback such as singularities. The body-fixed angular velocity vector and the Euler rate vector are related through a transformation matrix $J_2(\eta_2)$ which is undefined for a pitch angle of $\theta = \pm 90^0$. The Euler angles is obtained by three successive rotations about different axes, known as Euler angle sequence. Following Euler angle sequence is chosen to transform reference to body frame.

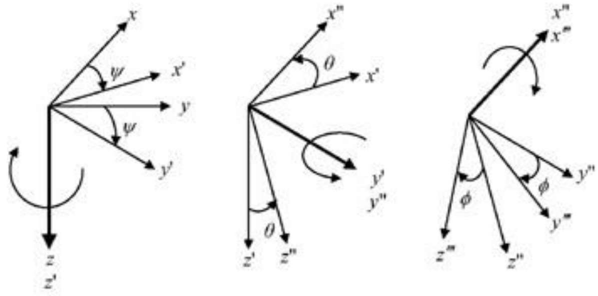

Fig. 4.2: Euler angle sequence.

- Rotate through angle $\psi(yaw)$ about reference z-axis.
- Rotate through angle $\theta(pitch)$ about reference y-axis.
- Rotate through angle $\phi(roll)$ about new x-axis.

The three rotations may be expressed mathematically by following three separate direction cosine matrices, respectively:

- Rotate ψ about z-axis, $C_z = \begin{bmatrix} c\psi & s\psi & 0 \\ -s\psi & c\psi & 0 \\ 0 & 0 & 1 \end{bmatrix}$ (4.1)
- Rotate θ about y-axis, $C_y = \begin{bmatrix} c\theta & 0 & -s\theta \\ 0 & 1 & 0 \\ s\theta & 0 & c\theta \end{bmatrix}$ (4.2)
- Rotate ϕ about x-axis, $C_x = \begin{bmatrix} 1 & 0 & 0 \\ 0 & c\phi & s\phi \\ 0 & -s\phi & c\phi \end{bmatrix}$ (4.3)

Thus, a transformation from reference to body axes may be expressed as product of these separate transformation as follows:

$$C_n^b = C_x C_y C_z$$

$$= \begin{bmatrix} c\psi c\theta & s\psi c\theta & -s\theta \\ -s\psi c\phi + c\psi s\theta s\phi & c\psi c\phi + s\psi s\theta s\phi & c\theta s\phi \\ s\psi s\phi + c\psi s\theta c\phi & s\psi s\theta c\phi - c\psi s\phi & c\theta c\phi \end{bmatrix} \tag{4.4}$$

Similarly, the inverse transformation from body to reference axes is given by:

$$C_b^n = \left(C_n^b\right)^T = \left(C_z\right)^T \left(C_y\right)^T \left(C_x\right)^T \tag{4.5}$$

b) Quaternion: An alternative to the Euler angle representation is a four-parameter method based on unit quaternion. It solve the Euler's singularity which is undefined for a pitch angle of $\theta = \pm 90^0$.

$$Q = \{q \mid q^T q = 1, q = [\eta, \varepsilon^T]^T, \ \varepsilon \in R^3 \ and \ \eta \in \square\} \quad \varepsilon = [\varepsilon_1, \varepsilon_2, \varepsilon_3]^T \tag{4.6}$$

$$q = \begin{bmatrix} \eta \\ \varepsilon_1 \\ \varepsilon_2 \\ \varepsilon_3 \end{bmatrix} = \begin{bmatrix} \cos\frac{\beta}{2} \\ \lambda \sin\dfrac{\beta}{2} \end{bmatrix} \in \square \tag{4.7}$$

Where the unit vector $\lambda = [\lambda_1, \ \lambda_2, \ \lambda_3]^T$ is:

$$\lambda = \pm \frac{\varepsilon}{\sqrt{\varepsilon^T \varepsilon}}$$

And $\varepsilon_1^2 + \varepsilon_2^2 + \varepsilon_3^2 + \eta^2 = 1$

The rotation matrix transform between the linear velocity vector in the inertial reference frame to the velocity in the body-fixed reference frame can be expressed as:

$$R_b^n(q) = \begin{bmatrix} 1-2(\varepsilon_2^2+\varepsilon_3^2) & 2(\varepsilon_1\varepsilon_2-\varepsilon_3\eta) & 2(\varepsilon_1\varepsilon_3+\varepsilon_2\eta) \\ 2(\varepsilon_1\varepsilon_2+\varepsilon_3\eta) & 1-2(\varepsilon_1^2+\varepsilon_3^2) & 2(\varepsilon_2\varepsilon_3-\varepsilon_1\eta) \\ 2(\varepsilon_1\varepsilon_3-\varepsilon_2\eta) & 2(\varepsilon_2\varepsilon_3+\varepsilon_1\eta) & 1-2(\varepsilon_1^2+\varepsilon_2^2) \end{bmatrix} \tag{4.8}$$

c) Transformation between Euler Angles and Quaternion:

$$\begin{bmatrix} \varphi \\ \theta \\ \psi \end{bmatrix} = \begin{bmatrix} a\tan\left(\dfrac{2\left(q_0q_1+q_2q_3\right)}{1-2\left(q_1^2+q_2^2\right)}\right) \\ a\sin\left(2\left(q_0q_2-q_3q_1\right)\right) \\ a\tan\left(\dfrac{2\left(q_0q_3+q_1q_2\right)}{1-2\left(q_2^2+q_3^2\right)}\right) \end{bmatrix} \tag{4.9}$$

$$\begin{bmatrix} \varphi \\ \theta \\ \psi \end{bmatrix} = \begin{bmatrix} a\tan 2\left(2\left(q_0q_1+q_2q_3\right),1-2\left(q_1^2+q_2^2\right)\right) \\ a\sin\left(2\left(q_0q_2-q_3q_1\right)\right) \\ a\tan 2\left(2\left(q_0q_3+q_1q_2\right),1-2\left(q_2^2+q_3^2\right)\right) \end{bmatrix}$$

d) Transformation between Quaternion and Euler Angles:

$$q = \begin{bmatrix} q_0 \\ q_1 \\ q_2 \\ q_3 \end{bmatrix} = \begin{bmatrix} \cos(\varphi/2)\cos(\theta/2)\cos(\psi/2)+\sin(\varphi/2)\sin(\theta/2)\sin(\psi/2) \\ \sin(\varphi/2)\cos(\theta/2)\cos(\psi/2)-\cos(\varphi/2)\sin(\theta/2)\sin(\psi/2) \\ \cos(\varphi/2)\sin(\theta/2)\cos(\psi/2)+\sin(\varphi/2)\cos(\theta/2)\sin(\psi/2) \\ \cos(\varphi/2)\cos(\theta/2)\sin(\psi/2)-\sin(\varphi/2)\sin(\theta/2)\cos(\psi/2) \end{bmatrix} \tag{4.10}$$

4.2 Kalman Filter

The Kalman filter is a set of mathematical equations that provides an efficient computational means to estimate the state of a process, in a way that minimizes the mean of the squared error. The filter is very powerful in several aspects: it supports estimations of past, present and even future states and it can do so even when the precise nature of the modeled system is unknown.[10]

The Discrete Kalman Filter Algorithm

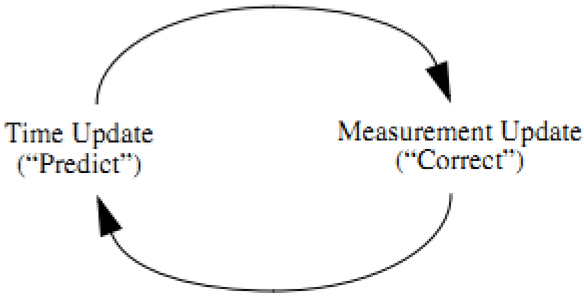

Fig. 4.3: The Discrete Kalman Filter Algorithm.

The equations for the Kalman filter fall into two groups: time update equations and measurement update equations. The time update equations are responsible for projecting forward (in time) the current state and error covariance estimates to obtain the a priori estimates for the next time step. The measurement update equations are responsible for the feedback- i.e. for incorporating a new measurement into the a priori estimate to obtain an improved a posteriori estimate.

The time update equations can also be thought of as predictor equations, while the measurement update equations can be thought of as corrector equations.

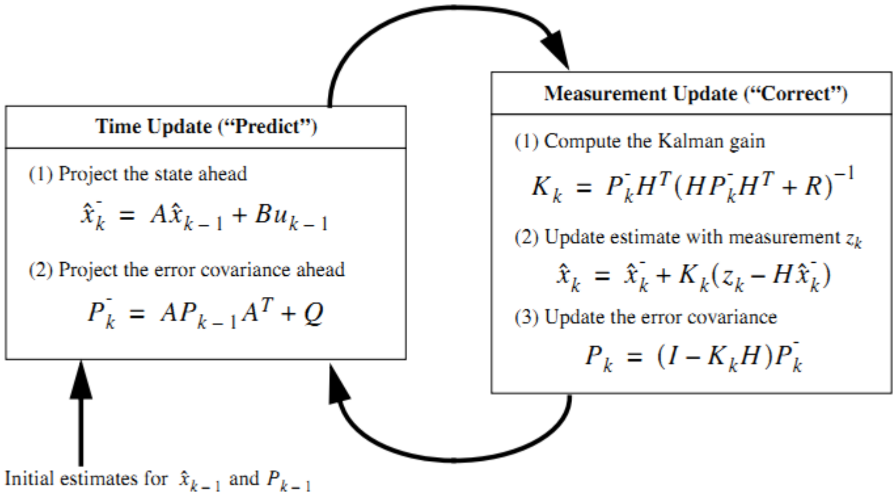

Fig. 4.4: The operation of the Kalman filter.

a) The time update equations projects the state and covariance estimates forward from time step k-1 to step k.

- The nxn matrix A in the difference equation (1) of time update equations relates the state at the previous time step k-1 to the state at the current step k, in the absence of either a driving function or process noise.
- The nxl matrix B relates the optional control input $u \in \mathbb{R}^l$ to the state x.
- The process noise covariance Q might change with each time step or measurement.

b) The measurement update:

- The first task is to compute the Kalman gain K_k.
- The next step is to actually measure the process to obtain z_k and then to generate an a posteriori state estimate $\hat{x}_k$

- Then final step is to obtain an a posteriori error covariance estimate via P_k

After each time and measurement update pair, the process is repeated with the previous a posteriori estimates used to project or predict the new a priori estimates.

4.3 Proportional Integral Differential (PID) control

PID's are essentially algorithms which are primary used in control application. These algorithms try to control the output of a system by minimising the difference or error between the setpoint (desired value) & current point (observed value). One of the classic application example of PID control would be the oven thermostat. The thermostat's primary function would be to maintain a certain temperature within the oven by varying the amount of heat the oven's heating element could give out in order the maintain the set temperature within the oven.

- P – Proportional Control
- I – Integral Control
- D – Derivative Control

These three terms are then multiplied by their respective constants and then summed up to give the final PID Control output.

$$PID = K_p.error + K_i.\int error\,dt + K_d.\frac{d\,error}{dt} \tag{4.11}$$

K_p: Proportional gain, a tuning parameter.

K_i: Integral gain, a tuning parameter.

K_d: Derivative gain, a tuning parameter.

$error$ = set point – current point.

t: Time or instantaneous time.

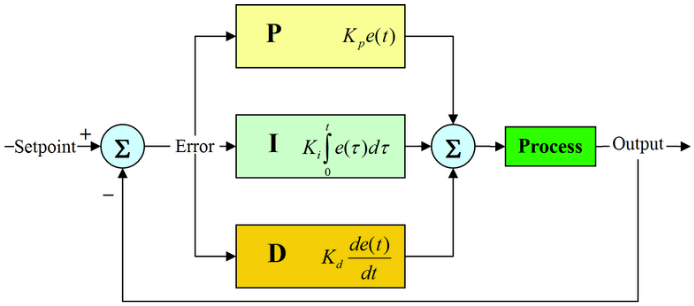

Fig. 4.5: A block diagram of a PID controller.

Table 4.1: PID tuning.

Method	Advantages	Disadvantages
Manual Tuning	No math required. Online method	Requires experienced personnel
Ziegler-Nichols	Proven method. Online method	Process upset, some trail-and-error, very aggressive tuning.
Software tools	Consistent tuning. Online or offline method. May include valve and sensor analysis.	Some cost and training involved

a) Manual tuning:

If the system must remain online, one tuning method is to first set K_i and K_d values to zero. Increase the K_p until the output of the loop oscillates, then the K_p should set to approximately half of that value for a "quarter amplitude decay" type reponse. Then increase K_i until any offset is corrected in sufficient time for the process. However, too much K_i will cause instability. Finally, increase K_d if required, until the loop is acceptably quick to reach its reference after a load disturbance. However, too much K_d will cause excessive response and overshoot. A fast PID loop tuning usually overshoots slightly to reach the setpoint more quickly; however, some systems can't accept overshoot, in which case an over-damped closed-loop systems is required, which will require a K_p setting significantly less than half that of the K_p setting causing oscillation.

Table 4.2: Effects of increasing a parameter independently.

Parameter	**Rise time**	**Overshoot**	**Settling time**	**Steady-state error**	**Stability**
K_p	Decrease	Increase	Small change	Decrease	Degrade
K_i	Decrease	Increase	Increase	Decrease	Degrade
K_d	Minor Decrease	Minor Decrease	Minor Decrease	No effect	Improve if K_d small

b) Ziegler-Nichols method:

As in the method above, the K_i and K_d gains are first set to zero. The K_p gain is increased until it reaches the ultimate gain, K_u , at which the output of the loop starts to oscillate. K_u and the oscillation period P_u are used to set the gains as shown:

Table 4.3: Ziegler-Nichols method.

Control Type	K_p	K_i	K_d
P	$0.5K_u$		
PI	$0.45K_u$	$1.2K_p\ /\ P_u$	
PID	$0.6K_u$	$2K_p\ /\ P_u$	$K_p P_u\ /8$

c) PID tuning software:

Most modern industrial facilities no longer loops using the manual calculation methods shown above. Instead, PID tuning and loop optimization software are used to ensure consistent results. These software will gather the data, develop process models, and suggest optimal tuning. Some software packages can even develop tuning by gathering data from reference changes.

Advances in automated PID loop tuning software also deliver algorithms for tuning PID loops in a dynamic or Non-Steady State (NSS) scenario. The software will model the dynamics of a process, through a disturbance, and calculate PID control parameter in response.

Chapter 5 Experiments and Results

5.1 Developed AHRS

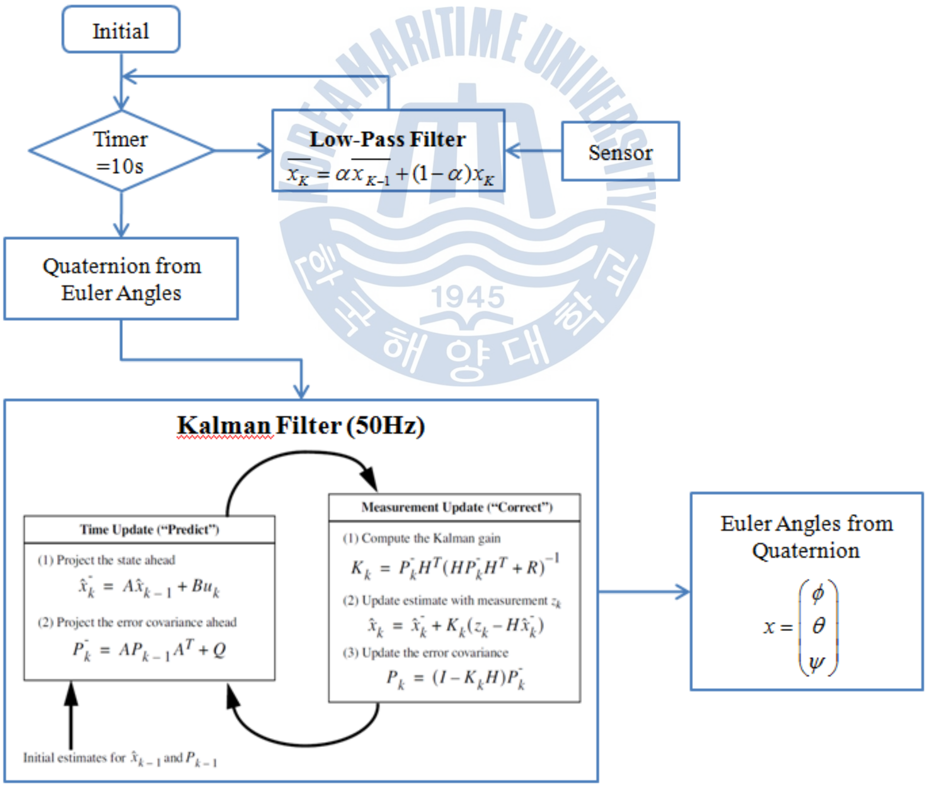

Fig. 5.1: Flow diagram of AHRS system.

Fig. 5.1 represents the flow diagram of AHRS system. Kalman filter needs the initial estimates which are as accurately as possible. Hence in first 10 seconds, just calculate the roll, pitch, yaw angles by using Low-pass filter and then transfer to quaternion from Euler Angles. After that apply Kalman with two steps: Predictor equations and Corrector equations to get the real attitude values.

The below figures will illustrate the attitude experiment results that include Roll, Pitch, Yaw angles before filter and after using Kalman filter. The data will be more accurate, with small error and nearly real signals. It will be better if we use more high-speed microprocessor as well as improve the loop time to 500Hz.

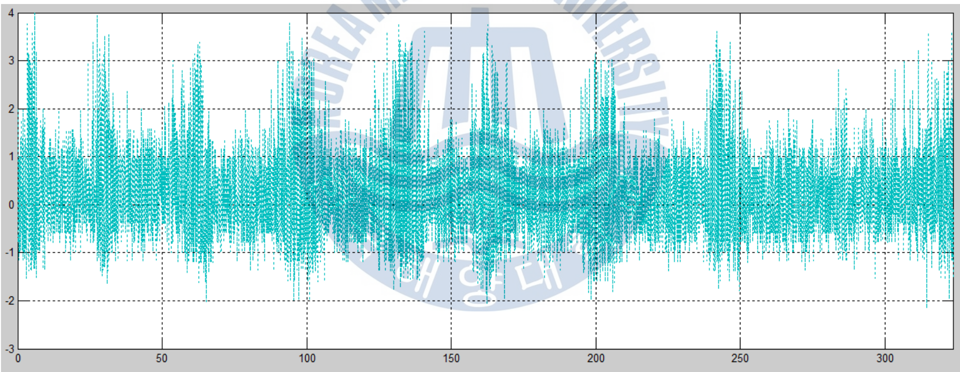

Fig. 5.2: Roll angle without filter (Max Error= 6°).

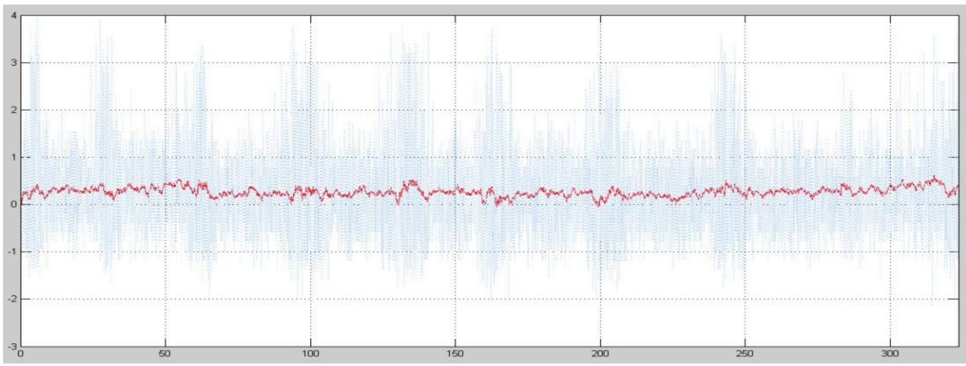

Fig. 5.3: Roll angle after filter (Max Error= 0.5°).

In Fig. 5.2 The output signal of Roll angle without Kalman Filter has many noise with Max Error= 6 degree. That isn't real value of body attitude. However, after through filter, the signal will be better, Max Error= 0.5 degree, and get approximately real value (Fig. 5.3).

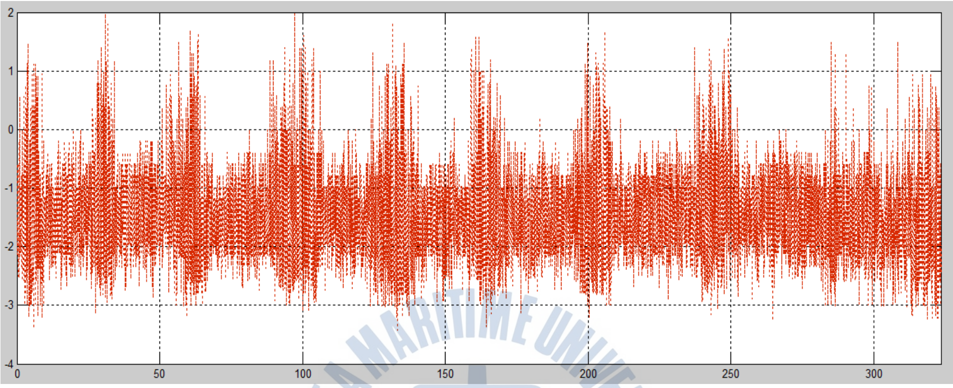

Fig. 5.4: Pitch angle without filter (Max Error= 5⁰).

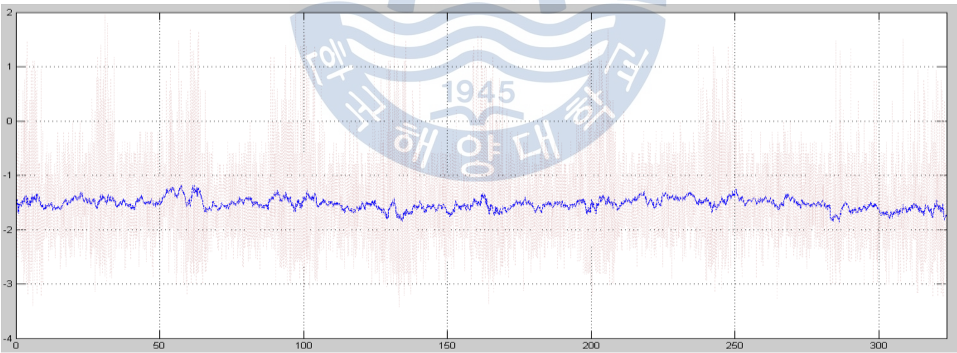

Fig. 5.5: Pitch angle after filter (error= 0.6⁰).

In Fig. 5.4 The output signal of Pitch angle without Kalman Filter has many noise with Max Error= 5 degree. That isn't real value of body attitude. However, after through filter, the signal will be better, Max Error= 0.6 degree, and get approximately real value (Fig. 5.5).

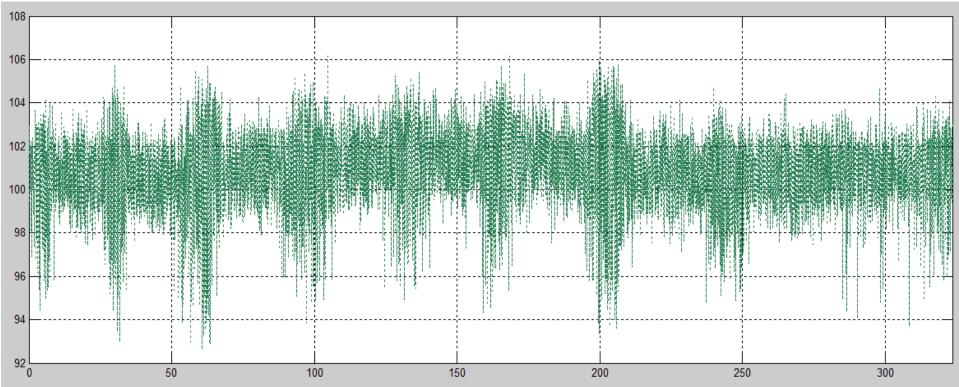

Fig. 5.6: Yaw angle without filter (Max Error= 12°).

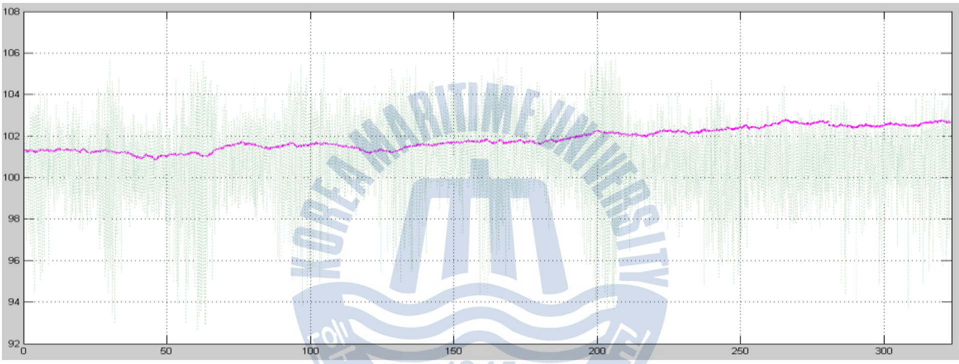

Fig. 5.7: Yaw angle after filter (Max Error= 1.5°).

In Fig. 5.6 the output signal of Yaw angle without Kalman Filter has many noise with Max Error= 12 degree. That isn’t real value of body attitude. However, after through filter, the signal will be better, Max Error= 1.5 degree. But it will be drifted by over time and not exactly like initial cases before.

5.2 UDR Experiments

5.2.1 Buoyancy

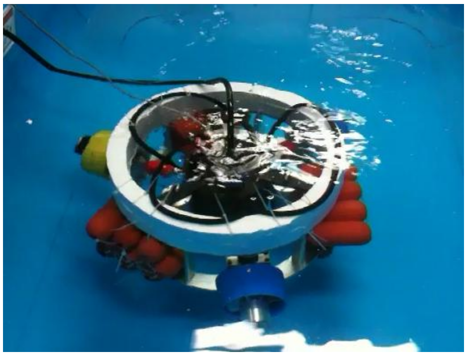

Fig. 5.8: UDR in water-tank.

For making buoyancy force, UDR is attached Styrofoam which will exterminate the UDR mass and always make floating without depth control. The Styrofoam volume is calculated by experiments. Fig. 5.9 and Fig. 5.10 show the result when it is floating in the water-tank with Roll angle, Pitch angle near 0 degree. It is convenient to control tilt, depth, and motion.

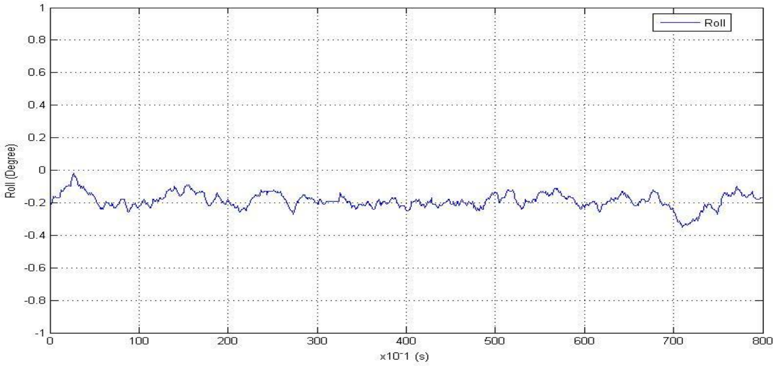

Fig. 5.9: The Roll angle.

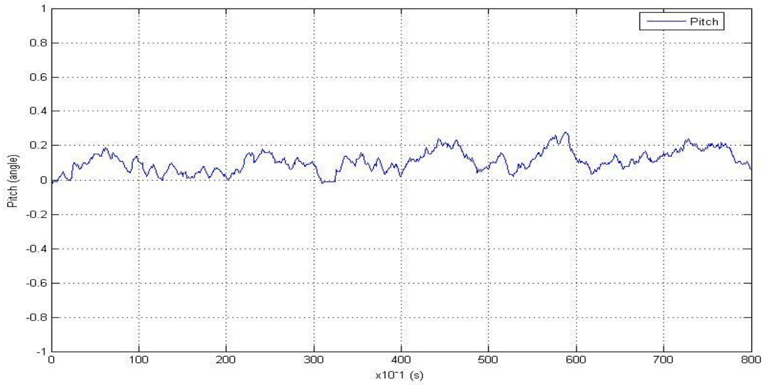

Fig. 5.10: The Pitch angle.

5.2.2 Tilt and Depth Control

$$u(t) = K_p.error + K_i.\int error\,dt + K_d.\frac{d\,error}{dt} \tag{5.1}$$

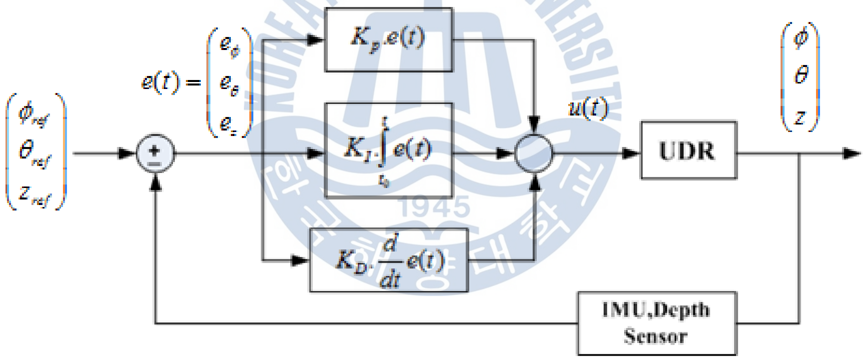

Fig. 5.11: PID for Title and Depth control.

PID Algorithm is used to control Tilt and Depth by three DC motors. This is so complex because DC motors are disposed symmetrically by 120 degrees. There are the interactions between rolling control with pitching control and depth control. With small change of roll angle will effect to pitch angle, depth and vice versa. First, the reference signals are compared with feedback signals which are measured by IMU sensor and depth sensor. After through PID controller, the output vector M will cause UDR quickly reach the desired position, orientation.

Fig. 5.12: Control Depth and keep Roll=Pitch=10 degree.

a) Experiment with Roll=Pitch=0 degree

$$K_p = 4.0;\ K_i = 0.2;\ K_d = 0.4$$

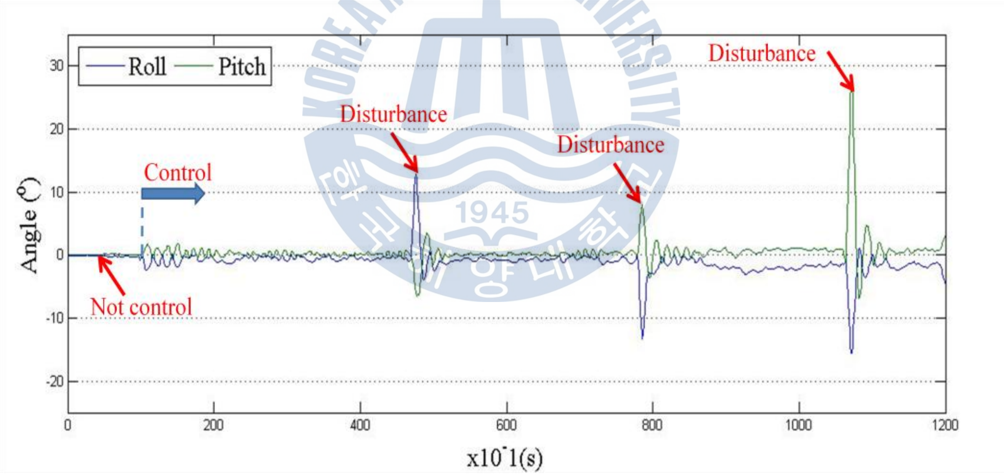

Fig. 5.13: Control Title to Roll=Pitch=0 degree with disturbance.

Fig 5.13 represents the UDR's attitude in two cases: not controlled and controlled in the disturbance environment. Without control, UDR maintains the free state with Roll and Pitch angle around 0 degree. Under the effect of disturbances, it will change the state and become unstable, oscillation. To put the system back to steady state before the PID algorithm is applied and it take some seconds.

b) Experiment with Roll=Pitch=0 degree, Depth=0.2m

$$K_p = 4.0;\ K_i = 0.2;\ K_d = 0.4$$

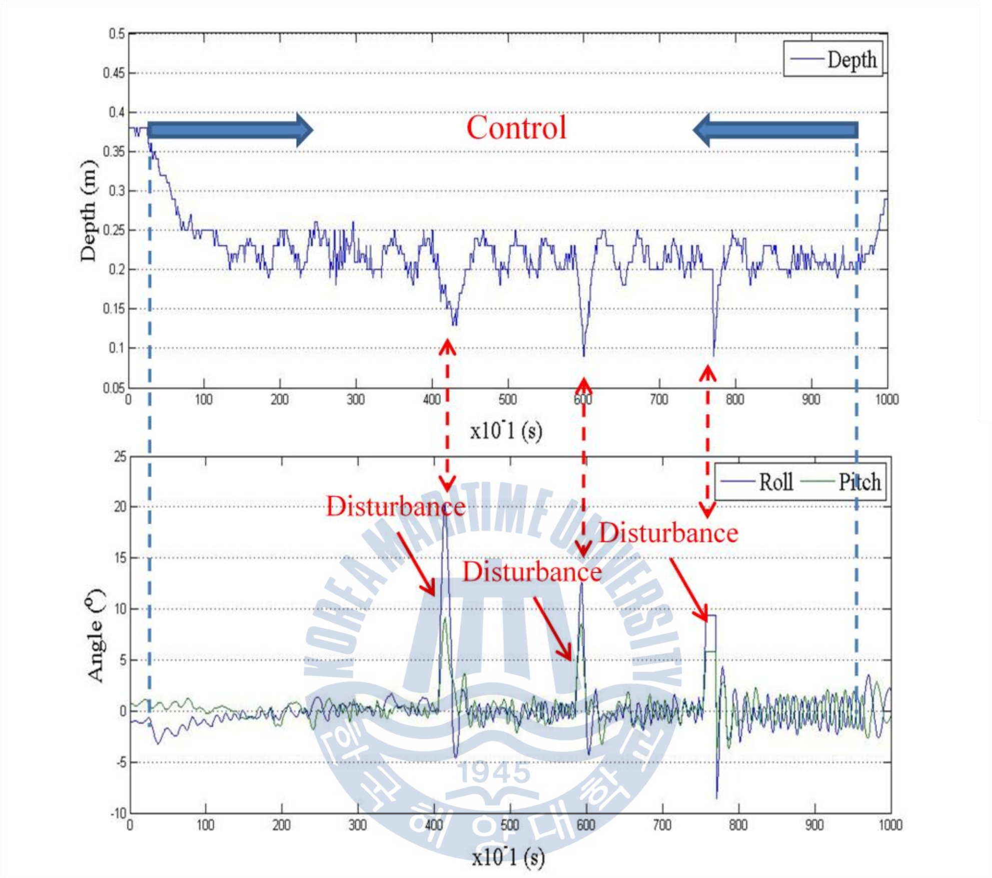

Fig. 5.14: Control Roll=Pitch=0 degree, Depth=0.2m with disturbance

Fig 5.14 represents the UDR's attitude in two cases: not controlled and controlled in the disturbance environment. We want to keep system in Roll=Pitch=0 degree and Depth=0.2m. When applied PID algorithm the UDR will quickly reach the desired state and maintain it stabilization. Under the effect of disturbances, the UDR will change the state and become unstable, oscillation. But it only exists in a few seconds and will return to steady state before by effect of the controller.

c) Experiment with Roll=Pitch=10 degree, Depth=0.2m

$$K_p = 4.0;\ K_i = 0.2;\ K_d = 0.4$$

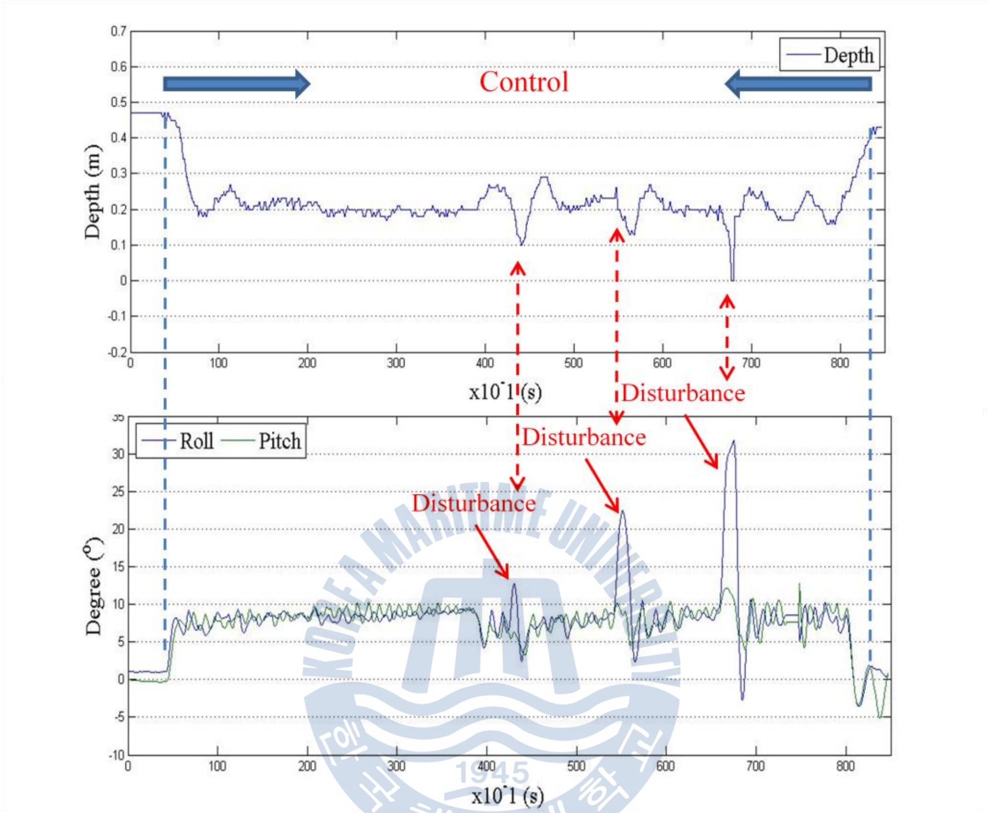

Fig. 5.15: Control Roll=Pitch=10 degree, Depth=0.2m with disturbance

Fig 5.15 represents the UDR's attitude in two cases: not controlled and controlled in the disturbance environment. We want to keep system in Roll=Pitch=10 degree and Depth=0.2m. When applied PID algorithm the UDR will quickly reach the desired state and maintain it stabilization. Under the effect of disturbances, the UDR will change the state and become unstable, oscillation. But it only exists in a few seconds and will return to steady state before by effect of the controller.

Chapter 6 Conclusion

In this paper, we designed a new UDR structure which can be less affected by external disturbances and operated swift motion to any direction by robust vector propulsion control scheme. Beside that, the control system is completely built with PID algorithm and Kalman filter. Initial experiments carried out good results about AHRS, buoyancy, depth and tilt test. In the next step, to complete and optimize system we need to add more sensors such as DVL, GPS, USBL for the navigation in the water and the surface. Increase the processing speed by using more high-speed microprocessor or embedded computer that will be easy to calculate and apply the complex algorithms.

References

[1] http://en.wikipedia.org/wiki/Main_Page

[2] Justin E. Manley, "Unmanned Surface Vehicles, 15 Years of Development", Proceedings of Oceans 2008, Quebec City, Canada, Sept.2008.

[3] Robert L. Wernli, "AUV'S -- THE MATURITY OF THE TECHNOLOGY", Proceedings of Oceans '99, MTS/IEEE, Seattle, WA , USA, September 1999.

[4] Roman, C.; Pizarro, O.; Eustice, R.; Singh, H. ," A new autonomous underwater vehicle for imaging research ", Proceedings of Oceans 2000, MTS/IEEE, vol 1, pp 153-156, September 2000.

[5] Thor I.Fossen, "Guidance and Control of Ocean Vehicles", John Wiley & Son, New York , 1994.

[6] www.ti.com, Texas Instrument .Inc.

[7] Tae-Hwan Joung, Han-Il Park, Sang-Young Lee, Moon-An Kim…," An Verify by Experimental Test for Estimation of Propulsion Performance of the Unmanned Underwater Vehicle ", Conference Proceedings of Korea Ocean Engineering 2011.

[8] Ngo Thanh Hoan, "A Study on a Low-Cost Attitude and Heading Estimation System for ROVs", Master thesis, Korea Maritime University, August 2008.

[9] D. H. Titterton, J. L. Weston, "Strapdown Inertial Navigation Technology", 2nd edition, American Institute of Aeronautics and Astronautics, 2004.

[10] Greg Welch, Gary Bishop, "An Introduction to the Kalman Filter", UNC-Chapel Hill, TR 95-041, July 24, 2006

[11] A. J. Baerveldt, R. Klang, "A low-cost and low-weight attitude estimation system for a autonomous helicopter", in Proc. 1997 IEEE Int. Conf. on Intelligent Engineering Systems, Budapest, Hungary, pp. 391-395, 1997.

[12] D. Jurman, M. Jankovec, R. Kamnik, M. Topic, "Calibration and data fusion solution for the miniature attitude and heading reference system", Sensors and Actuators, pp. 411-420, 2007.

[13] P. Zarchan, H. Musoff, "Fundamentals of kalman filtering: A practical approach", American Institute of Aeronautics and Astronautics, 2005.
[14] B. Barshan, H.F. Durrant-Whyte, "Inertial navigation systems for mobile robots", IEEE Transactions on Robotics and Automation, vol.11, no.3, 1995.
[15] US Navy, "The Navy Unmanned Undersea Vehicle (UUV) Master Plan", November 9, 2004, p.67.
[16] J.Yuh, "Learning Control for Underwater Robotic Vehicles", IEEE International Conference on Robotics and Automation, Atlanta, GA, May 1993.
[17] Podder, Tarun K., G. Antonelli, and N. Sarkar, "Fault-Accommodating Thruster Force Allocation of an AUV Considering Thruster Redundancy and Saturation", IEEE Transaction on Robotics and Automation, April 2002.
[18] Yasuyuki Kataoka, Kazuma Sekiguchi, MitsujiSampei, "Nonlinear Control and Model Analysis of Trirotor UAV Model", the 18th IFAC World Congress, Milano (Italy) August 28 - September 2, 2011.
[19] GabrielM. Hoffmann, Huang,H.S.L.W. and Tomlin,C.J. (2007). "Quadrotor helicopter flight dynamics and control:Theory and experiment". Proc. Of AIAA Guidance, Navigation and Control Conference and Exhibit.
[20] Ian C. Rust and H. Harry Asada, " The Eyeball ROV: Design and Control of a S pherical Underwater Vehicle Steered by an Internal Eccentric Mass", IEEE International Conference on Robotics and Automation, Shanghai, China, May 9-13, 2011.